SLURRY PHASE IRON CATALYSTS FOR INDIRECT COAL LIQUEFACTION

Semi-Annual Technical Report

Reporting Period: July 4, 1996 - January 5, 1997

Author: Abhaya K. Datye

Report Issue Date: February, 1997

DE- FG22-95PC95210

University of New Mexico
Center for Microengineered Materials
Albuquerque, NM 87131

Disclaimer

Abstract

This report describes research conducted to support the DOE program in indirect coal liquefaction. Specifically, we have studied the attrition behavior of iron Fischer-Tropsch catalysts, their interaction with the silica binder and the evolution of iron phases in a synthesis gas conversion process. The results provide signficant insight into factors that should be considered in the design of catalysts for converting coal based syn-gas into liquid fuels.

Table of Contents page

Technical Progress

Executive Summary

This report covers the third six months of this three year grant under the University Coal Research program. During this period, we have explored the uniaxial compaction method as an approach to derive particle breaking stress. The method was applied to alumina support granules obtained from Dr. Robert Gormley at PETC and will be extended to other F-T catalysts in future work. We also present ultrasonic fragmentation analysis of Fe/alumina F-T samples obtained from PETC. When the particle size evolution is compared with that of the base UCI catalyst, it is clear that the alumina-supported catalysts show significant improvement in particle strength. This work will be continued over the next six month period to better quantify the agglomerate strength of F-T catalysts, and to afford comparisons between the uniaxial compaction and ultrasonic fragmentation methods for determining the strength of F-T catalysts.

During this period, we have continued our study of Fe/silica interactions to provide a fundamental understanding of the how silica binders influence the activity and attrition resistance of these catalysts. To understand differences in the reducibility of the iron phase caused by silica, we have set up a temperature programmed reduction facility. TPR in H_2 as well as in CO was performed of Fe/SiO_2 catalysts prepared by impregnation as well as by precipitation.

We have completed analysis of catalysts received from slurry reactor runs at Texas A&M university (TAMU) and the University of Kentucky Center for Applied Energy Research (CAER) by x-ray diffraction. The analysis results were conveyed to PETC, TAMU and CAER in September 96 are included here for the sake of completeness. The purpose of the XRD analysis was to determine the phase composition of catalysts derived from a slurry reaction run using Fe Fischer-Tropsch catalysts. As we describe in this report, the XRD results show that the carbide phase *does not* transform into magnetite over the course of a F-T run, both in the TAMU as well as in the CAER runs. The slow deactivation of these catalysts must then be related to crystallite growth and loss of active phase surface area. Further work is underway to corroborate this hypothesis.

Technical Objectives

The objective of this research project is to perform fundamental research in support of catalyst development for slurry phase bubble column reactors for Fischer-Tropsch synthesis. The overall program is divided into the following tasks:

Task 1. Catalyst Particulate Synthesis
Task 2. Catalyst Binder Interactions.

In task 1, we will first study factors that determine the attrition resistance of slurry phase Fe catalysts. Fundamental understanding of the attrition phenomenon will be used to guide the synthesis of novel precipitated catalysts that overcome some of the limitations of current generation catalysts. The investigation of catalyst microstructure as a function of treatment will help determine the optimal treatment protocols for F-T synthesis catalysts. Since the use of binders is considered essential for providing the desired attrition resistance, the second task is to perform fundamental studies of catalyst-binder interactions. These studies will use model catalysts that can be studied by high resolution transmission microscopy to investigate the nature of interfacial phases at the Fe-binder interface. A better understanding of the phenomena that lead to catalyst-binder interactions will help us design improved catalysts for indirect coal liquefaction.

Task 3. Characterization of catalysts received from CAER, Univ. of Kentucky, and from Texas A&M.

Task 3 was not included in our original proposal. However, we are pursuing these studies to help understand catalyst deactivation under actual reaction conditions.

Technical Progress

Task 1: Catalyst Particulate Synthesis

Overview

In the previous six-monthly report we showed how ultrasonic excitation followed by sedigraph particle size distribution can yield a simple test for the strength of catalyst agglomerates. While the breakdown of particles subjected to ultrasound energy provides a graphic measure of particle strength, a number of assumptions must be made to derive a quantitative measure of particle strength. Hence, during the current six month period we have explored the use of a more conventional test for particle strength.

Uniaxial Compression Testing

Uniaxial compression testing is a technique for characterizing the strengths of powders and granular materials. Previously, the conventional method used for compression tests was the “Brazilian test”, in which individual particles were crushed between two platens (1). The drawback to this method was in the variability of strength due to variations of individual particle sizes and shapes. Furthermore, individual particle fracture loads are small (equivalent to a few grams’ weight) such that the accuracy of the data might not be high.

A simple alternative method consisted of replacing the individual particle with a confined bed of similar particles, inferring some average individual particle strength parameter from the behavior of the whole bed under compression (1). This method is easily achieved using a piston in a cylinder, hence this method involves a uniaxial compaction (as shown on the next page).

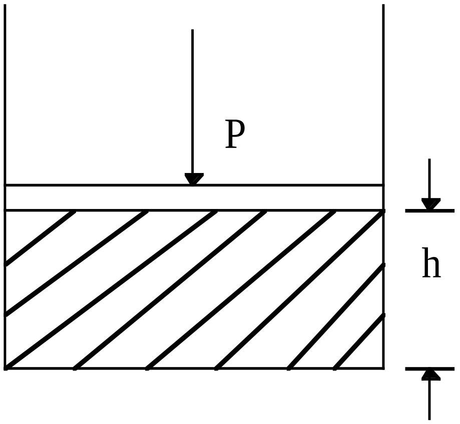

Confined Uniaxial Compression Test

Uniaxial compression testing has been used by a group at Sandia National Laboratories in the study of ceramic granule strength. The tests were performed at the Advanced Materials Laboratory (a joint Sandia National Labs- University of New Mexico facility located on the university research park). For comparison, uniformly sized glass spheres were also used in their study. Diametral compression strength tests, similar to the "Brazilian test", were performed (2) and the results were compared with those obtained with the uniaxial compaction test. The uniform-size glass spheres were used to eliminate the effects of shape and size factors, and minimize strength variability. Surprisingly, the results showed that the glass spheres also exhibited large variability in strength. The results for ceramic granules and uniform-size glass spheres were verified by using Weibull statistics; indeed, results the glass spheres gave similar Weibull parameters to those obtained from ceramic granules, indicating a large strength variability for individual glass spheres. Although the glass spheres were uniform in size, the large variability in strength was thought to arise from the large range in flaw sizes.

To circumvent the tedious task of testing individual granules by the diametral compression test, pressure compaction (P-C) tests were also performed by Jill Glass and coworkers at SNL. Compaction behavior of these samples was determined by plotting the relative density of the compacted sample vs. the log of the compaction pressure as shown on the next page (2).

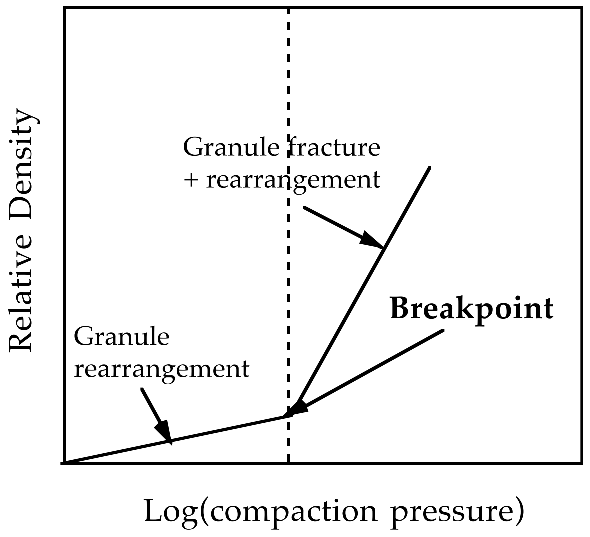

This figure shows how the data of relative density vs log pressure can provide a semi-quantitative measure of agglomerate strength. As shown in this plot, compaction data tend to exhibit linear regimes that can be attributed to different compaction mechanisms (3). In the first regime, the gradual increase in relative density is due to particles, such as granules and agglomerates, sliding and rearranging without fracture. At this stage little compaction occurs, and only a small percentage of the void space is removed during rearrangement. It is often observed experimentally that this regime has a slope of ≈0.003-0.005. In the second regime, a sharp increase in relative density is due to deformation and fracture in conjunction with the sliding and rearrangement of particles (slope ≈ 0.2). At this stage a larger percentage of void space is removed during rearrangement. Best fit lines are often drawn through the points in the two linear regimes of the compaction plot. The intersection of these lines is called the breakpoint, which acts as a transition point for the two regimes. The breakpoint has been used as a semi-quantitative indicator of powder/granule strength or yield point, and is thought of as the average strength. Recent work at SNL, however, has demonstrated that it is more representative of the lower end of the range of powder or granule strengths. Beyond the second regime there may be another characteristic slope at higher pressures, but this has not been analyzed because it is still not well understood.

In our work, we have explored the use of uniaxial compression testing to measure the strengths of Fischer-Tropsch catalysts. An Instron 5565 machine was used for compaction tests of these catalysts. This machine allows different-size dies to be used depending on the amount of samples available. We have chosen to work with an 1/8″ die to minimize the amount of sample required for a given test.

Experimental Details

A sample of VISTA-B-965-500C (Alumina), obtained from Dr. Robert Gormley at the Pittsburgh Energy Technology Center (PETC), was used for the uniaxial compression testing. Ten milligrams of this sample were loaded into the cell of a die with a 1/8″ opening. A plunger was then placed on top of the filled die, taking great care not to compress the sample. To account for the error due to deformation of the top plunger and to the compliance of the crosshead, the displacement of the empty fixture as a function of load was subtracted from the displacement of the filled die.

Compression tests were conducted by placing the filled die underneath the crosshead of the Instron machine. The crosshead was manually lowered such that it was just touching the top plunger. The displacement gauge was zeroed, and the crosshead was then activated at a rate of 1.00 mm / min. Testing was continued until a load of 1000 N was reached. The sample was repeated for reproducibility. For the first experiment, the sample was compacted at an aspect ratio, L_f/D of 0.61 (where L_f = final compact height and D = compact diameter); for the second experiment, the sample was compacted at an aspect ratio of 0.74.

Results

Figures 1 and 2 show plots of relative density vs. log of compaction pressure for the alumina. The relative density was calculated using the mass of alumina, initial compact height, measured displacement, and theoretical density. As expected, a low increase in relative density with an increase in pressure was followed by a region of sharp increase in relative density with pressure. The breakpoint was estimated by using best fit lines for the linear regimes and estimating the breakpoint via intersection of the lines. The breaking strength was determined to be 11.97 MPa from Fig. 1. The test shown in Fig. 2 yielded a curve that is almost identical to that of Fig. 1 up to 30 Mpa, but a lower slope at high loads yields a breakpoint of 6 MPa. Previous work by Jill Glass and coworkers (3) shows that as long as the aspect ratio L_f/D is maintained to be $\leq$ 1.2, , consistent compaction results will be produced. Although the same amount of alumina was used for both experiments (i.e., 10 mg), the aspect ratios were not the same due to factors such as individual particles sizes and shapes, the place at which the samples were taken from the sample in the bottle, and the disturbance of the sample in the die during placement of the top plunger. Further work is necessary to improve the data analysis procedure so that consistent results on particle breaking strength can be obtained. Once a consistent analytical procedure has been worked out, future work will involve a study of various Fischer-Tropsch catalysts to investigate how the binder morphology and loading affects the catalyst strength.

Ultrasonic fragmentation tests of F-T catalysts

Figs. 3-5 provide fragmentation analysis of three of the catalysts also obtained from Dr. Robert Gormley at PETC. Fig. 3 shows the break down of a UCI catalyst that was synthesized for La Porte run 1, and used for comparison with the alumina in this study. Figure 3 shows that 15 minutes of ultrasonic excitation at an amplitude of 20 (20% of full scale) results in significant production of fine particles. This result is comparable to that reported by us in our previous six-monthly report where additional details on the ultrasonic fragmentation method can be found. The analysis of the Vista alumina granules is shown in fig. 4 where we find very little breakdown of the catalyst with comparable ultrasound energy. This alumina powder is the same one used for uniaxial compaction analysis and its compaction curve is shown in Figs. 1 and 2. Fig. 5 presents ultrasonic fragmentation results from a catalyst prepared by depositing iron on the preformed alumina granules. As expected, particle breakdown is comparable to that of the blank alumina, and the catalyst appears much stronger than the base UCI catalyst.

Future Work

These results show that the uniaxial compaction and ultrasonic fragmentation tests may provide a good measure of the attrition resistance of F-T catalysts. Our future work will be devoted to developing consistent data analysis procedures for the compaction test and then comparing the ultrasonic fragmentation and compaction test results to the performance of catalysts in a slurry environment. We will expand the scope of these studies to include samples obtained from CAER and TAMU. During the course of this work, we will continue to study the microstructure of these catalysts to elucidate the role of binder morphology and loading on catalyst particle strength.

Task 2 - Catalyst-binder interaction

Overview

The focus of the work performed during this period was temperature programmed reduction of supported and unsupported catalysts to study how the binder-catalyst interaction affects the reducibility of the iron phase.

Experimental

Two silica sphere supported iron catalysts, YJ/1-65A(20 wt % Fe, with 1 wt % Cu) and YJ/1-67(10 wt % Fe), were prepared by conventional incipient wetness impregnation and precipitation respectively. A UCI unsupported catalyst (1185-149, $Fe_2O_3/CuO/K_2O = 88.95/11/0.05$) was used as a reference. In this study, a 10% CO/He or 10% H_2/Ar reductant stream was used with 20-30 mg catalyst sample contained in a U-shaped quartz reactor. A Thermal Conductivity Detector (TCD) was used for the analysis. An in-line CO_2 trap or H_2O trap located between the reactor and the detector was used to remove CO_2 or H_2O formed during TPR process. The sample temperature was ramped in each experiment at 10 °C /min to 500°C and then held at the latter temperature for 0.5-1 hour.

Results

Following an optimized TPR procedure, H_2-TPR profiles were recorded for unsupported UCI-1185-149 catalyst where the effect of preconditioning, i.e. heating in flowing Ar at the specified temperature, was first explored (see Fig. 6). Following each TPR, the sample was oxidized at 500 °C and a second TPR was performed. The 2nd run TPR profiles were quite similar, independent of the preconditioning procedure, hence only one curve is shown for the 2nd TPR run (curve d in fig. 6). Precalcination has appreciable effects on the TPR profile of unsupported UCI-1185-149, the lower temperature peak splits to three smaller peaks after 500°C precalcination. Presumably, the higher precalcination temperature causes agglomeration of the catalyst particles and pore structure collapse. This catalyst exhibits three distinct peaks in the 2nd TPR, presumably corresponding to reduction of CuO to Cu, Fe_2O_3 to Fe_3O_4, and Fe_3O_4 to Fe respectively. Phase separation of copper from iron is very likely to have occurred during the 1st run H_2-TPR, which causes the early reduction peaks to spread out and shift to higher temperature. Hence, some of the synergism between the Cu and Fe may not be seen in the 2nd TPR run. Changes in surface area and particle size could also account, in part, for this shift to higher reduction temperatures.

Fig. 7 shows the H_2-TPR results for sample YJ/1-65A, the (20 wt % Fe, 1 wt % Cu) catalyst prepared by impregnation. The effect of preconditioning (i.e. heating in flowing Ar) is much less pronounced than the unsupported catalyst. All the H_2-TPR profiles of supported catalysts exhibit three distinct peaks, almost not affected by the precalcination temperature. The 2nd-run also does not show significant peak shift from the 1st-run. The only major difference is that the ratio of the two low temperature peaks has changed. From the peak area ratio of the second run TPR profile, we again infer that the smaller peak to corresponds to the reduction of CuO to Cu, and the larger one for the reduction of Fe_2O_3 to Fe_3O_4 (the calculated hydrogen uptake ratio is 1/3.8 which agrees with the peak area ratio of the two low temperature peaks). It is likely that some phase separation of copper from iron also happens, as in the case of unsupported catalyst, resulting in the changes in peak shape. Our preliminary peak assignment is as follows: the first peak represents an overlap of the peaks corresponding to reduction of CuO to Cu and Fe_2O_3 to Fe_3O_4, the second one represents the transformation of unpromoted Fe_2O_3 to Fe_3O_4, and the broad higher temperature peak corresponds to conversion of Fe_3O_4 to Fe.

Fig. 8 presents H_2-TPR runs for two reference samples: commercial magnetite and a physical mixture of the UCI catalyst with silica sphere support. The high temperature peak of the commercial magnetite sample is similar to the high temperature peak of the physical mixture confirming that this corresponds to the Fe_3O_4 to Fe reduction step. The first TPR run of the physical mixture is different from that of the unsupported catalyst by itself, shown in Fig. 6. This suggests that the presence of the silica support by itself causes some of the peak position shifts and a chemical interaction may not necessarily be occurring.

CO-TPR

Two sets of CO-TPR profile were also recorded for supported and unsupported catalysts (Fig. 9 and 10). Once again, a comparison of the 1st and 2nd run provides evidence for catalyst sintering. For example, fig. 9b shows a sharp peak at low temperatures which is missing in the second run. We suspect this is caused by a synergistic reduction caused by the presence of CuO in contact with the iron oxide, but phase segregation after the high temperature reduction may cause the reduction peak to shift to higher temperatures in the 2nd TPR run. The impregnated Fe/SiO_2 catalysts shows very little effect of the high temperature reduction implying that silica helps to preserve the iron surface area in the catalyst. Furthermore, the area of the low temperature peak is much larger than even the unsupported catalyst, both in the 1st and the 2nd runs. Apparently, we cannot simply assign this peak to Fe_2O_3 reduction to Fe_3O_4. We suggest that, in case of supported catalyst, carburization or carbon deposition happens during reduction of Fe_2O_3 to Fe_3O_4.

Future Work

We find that comparison of the 1st and 2nd run profiles of the unsupported catalyst shows that the position of the peak corresponding to Fe_2O_3 to Fe_3O_4 is significantly changed for both H_2 as well as CO-TPR. This could be caused by severe sintering of the catalyst during the 1st-run TPR as well as phase segregation of copper from iron. While the promotion effect of copper on the reduction of iron catalysts has been seen in previous work, the effect of the copper on the formation of carbide phases is not well understood. In future work, we will examine the microstructure of catalysts removed at various stages of the TPR runs to help answer some of these questions, particularly the role of Cu and the nature of interaction of the iron oxide phase with the silica support.

Task-3: Characterization of catalysts from Univ. of Kentucky & Texas A&M

Overview

The analysis of samples obtained from CAER and TAMU over the course of a continuous F-T run are presented below.

XRD analysis of samples in wax from run SB-3425 performed at TAMU

An XRD pattern of natural magnetite is enclosed for reference **(Fig. 11)**.

TOS=000 hrs **(Fig. 12)**. This sample contains predominantly α-Fe with a very small amount of Fe_3O_4. As indicated by the Reitveld analysis, the fit to α-Fe is very good. The residual after fitting the α-Fe is magnetite. From the broad peaks, it would appear to have a small particle size.

TOS=111hrs **(Fig. 13)**. The major peaks are those due to Fe-carbide between 2.271 Å - 2.108 Å. A small peak is seen at 2.483. In the reference magnetite sample the prominent peak appears at 2.523 Å. I am not sure if the 2.483 Å peak should be assigned to magnetite or whether it is just one of the carbide peaks. The natural magnetite sample was analyzed as a powder while these samples are in the wax. I am not sure if this would cause a peak shift, however it should be noted that the small α-Fe peak appears at its expected position.

TOS=233hrs **(Fig. 14)**. The pattern is very similar to that at TOS 111 hrs.

TOS=330 hrs **(Fig. 15)**. There are two significant changes in this pattern. The peak at 2.226 has disappeared while the peak at 2.984 has diminished in intensity. Second, the peak intensity of the major carbide peaks at 2.267 Å and 2.107 Å has increased. The latter means that the carbide is better crystallized or has grown in particle size. Interpretation of these patterns will have to await complete Reitveld analysis.

TOS=384hrs **(Fig. 16)**. This pattern is similar to that at 330 hours.

Summary

Over the 400 hours of running in an FT synthesis reactor, there is no apparent transformation of the carbide into magnetite even though the CO conversion is 80%. The slight deactivation seen at 330 hours may be attributed to the increased peak height of the carbide peaks (increased crystallinity, loss of surface area) and could also be possibly related to the disappearance of the peak at 2.226 Å and 2.984 Å This may suggest transformation of one form of carbide into another.

XRD analysis of samples in wax from run RJO-189 performed at CAER

We have analyzed the catalyst samples from this run that are embedded in wax. Since, there is an overlap between carbide and magnetite peaks at around 2.1 Å, we have used Reitveld analysis to strip the magnetite peaks from the spectrum. In this way, the carbide peaks can be clearly identified and the phase transformations from carbide to magnetite better understood.

Fig. 17 is an XRD powder pattern of magnetite that has been Reitveld refined to show how well the refinement procedure accounts for the intensities of the various magnetite peaks.

RJO-189F TOS=20h **(Fig. 18).** Fast scan of sample RJO189F. There was not enough sample left to do a step scan after the initial exploratory fast scan. Prominent magnetite peaks seen.

RJO-189G TOS=122h **(Fig. 19)**. Reitveld refinement for magnetite.

RJO-189G TOS=122h **(Fig. 20)**. Residual plot after Reitveld refinement for magnetite. The magnetite peaks have been subtracted and the residual shows carbide peaks at 2.177 and 2.073 Å. There are also less intense peaks at 1.481 Å, 1.276 Å and 1.090 Å.

RJO189J TOS=888 h **(Fig. 21)**. Slow scan XRD pattern of RJO189J. The magnetite peaks are fit by Reitveld refinement and the residual carbide pattern is shown at the bottom. There is a problem with the background subtraction that yields a negative peak at 2.968 Å. Overall, the peak intensity for both the carbide and magnetite peaks has increased suggesting that the sample is becoming more crystalline.

RJO 189J TOS=888 h **(Fig. 22)**. Residual plot after subtraction of the magnetite peaks. Carbide peaks are seen at 2.106 Å, 2.171 and 2.423 Å.

RJO 189M TOS=1796 h **(Fig. 23**). Step scan pattern for RJO189M.

RJO 189M TOS=1796 h **(Fig. 24)**. Residual after subtraction of magnetite. An additional peak is seen at 2.027 that is suggestive of the presence of α-Fe.

RJO 189M TOS=1796 h **(Fig. 25)**. The spectrum of RJO189M after Reitveld refinement for magnetite and α-Fe. The additional peak is confirmed to be α-Fe.

RJO 189P TOS=3547 h **(Fig. 26)**. Step scan of RJO189P. The peak intensity is much greater than on sample RJO189F indicating better crystallinity of the sample.

RJO 189P TOS=3547 h **(Fig. 27)**. This shows the raw data, fit for magnetite and the residual after subtracting magnetite.
RJO 189P TOS=3547 h **(Fig. 28)**. The XRD pattern is Reitveld refined for Cu but the fit is not good and negative peaks result indicating that there is no metallic Cu in this sample.

Summary

The full width at half maximum of the magnetite peak does not change significantly over the course of this run. This implies that there is no appreciable coarsening or grain growth of the magnetite phase. Examination of the peak areas of various magnetite peaks shows that the relative size of the peak at 2.099 is greater than that in the natural magnetite sample. This is due to overlap between the carbide and magnetite. As a first guess, these results would indicate that there is no significant transformation of carbide into magnetite over the course of the 3000 hour run. Had there been a transformation, the magnetite peak ratios should have approached those of natural magnetite as carbide was progressively converted into magnetite. There are important differences between the XRD patterns of these samples and those from the run performed at Texas A&M despite similarities in the operating conditions and pretreatment:

1. There are significant amounts of magnetite in the CAER samples while the amount of magnetite in the Texas A&M samples is negligible. The wax removal at Texas A&M is performed under an inert blanket while an inert blanket is not used during removal of the hot wax at CAER for this particular run. The role of the wax removal procedure on the relative amounts of magnetite and carbide need to be explored. The carbide peaks are well defined and show more lines than those in the CAER samples. Is this a result of these being different carbides or is it caused by difference in the extent of oxidation. We also do not have a sample of the catalyst after reduction and therefore do not know the extent of transformation to α-Fe during the reduction step. It would help to obtain a sample of this catalyst after the 220 °C H_2 activation so we could determine the phases present at the start of the run. If this reduction is performed for generating this sample, it would be useful to obtain sample with and without an inert blanket during discharge of the hot wax so that we can get an assessment of the extent of catalyst oxidation during wax discharge.

2. The loss of activity seems to be related to the increased crystallinity of the sample with time on stream. The peak intensity appears to increase with the XRD peaks becoming more well defined. This could be a result of the crystallite growth which would lead to loss of surface area. The peak widths of the magnetite peak do show a slight decrease in peak broadening with time on stream. However, at these particle sizes, particularly with the possible effects of lattice strain in the carbide, it may be best to resort to TEM analysis to infer the particle size changes.

Future Work

In future work, we will examine the wax stripped samples from these runs to derive detailed morphological information by electron microscopy.

We would like to obtain from CAER a sample in wax after H_2 treatment under the conditions used in this run with and without an inert blanket. This will allow us to assess the extent of catalyst oxidation during wax removal and also establish the initial phase composition of this catalyst.

Acknowledgments

The following graduate and undergraduate students participated in this project:
Linda Mansker, x-ray diffraction; Yaming Jin, F-T reactor studies and TPR; Aree Hanprasopwattana - catalyst synthesis and surface coatings; Hien Pham - attrition resistance studies. We also acknowledge helpful discussions with Dr. Mark Miller of the Earth and Planetary Sciences on Reitveld refinement methods for analysis of x-ray diffraction patterns and with Dr. Tom Rieker of the Chemical and Nuclear Engineering Department for assistance with small angle x-ray studies of titania/silica catalysts. The TEM and XRD measurements were performed using the analytical facilities provided by the Earth and Planetary Sciences Department.

References

1) M. J. Adams, M. A. Mullier, and J. P. K. Seville, *Powder Tech.*, **78** (1994) 5.
2) S. J. Glass, K. G. Ewsuk, and M. J. Readey, SAMPE Technical Conference, Albuquerque, NM, Oct. 9-12, 1995.
3) S. J. Glass and C. Newton, Symposium on Science, Technology, and Commercialization of Powder Synthesis and Shape Forming Processes, American Ceramic Society, Cincinnati, OH, 1995.

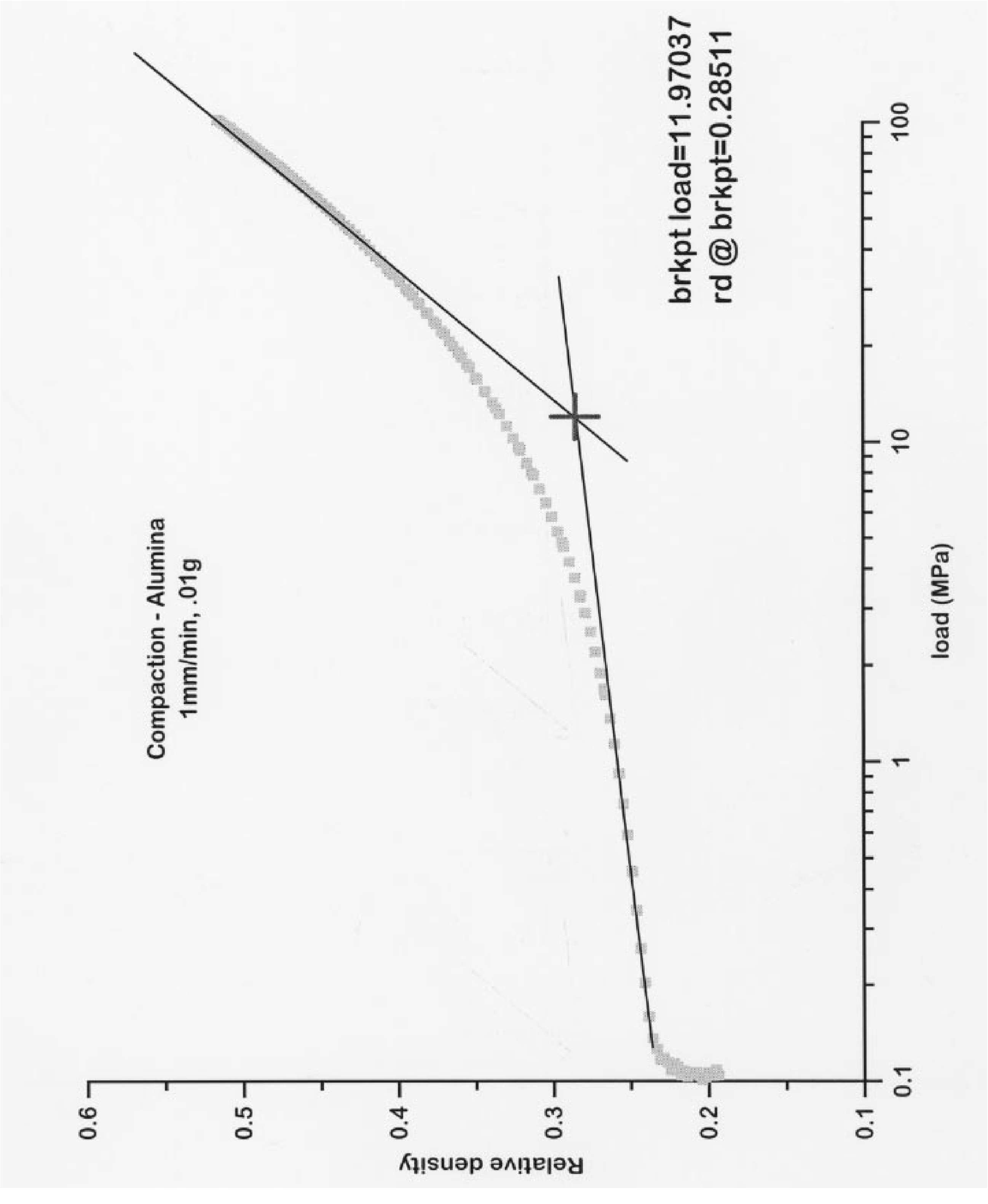

Fig. 1 Uniaxial compaction results for the Vista alumina sample VISTA-B-965-500C obtained from Dr. Robert Gormley. The relative density vs log P curve can be fit by two linear segments whose intersection determines a nominal breaking strength (11.97 MPa) for the alumina granules.

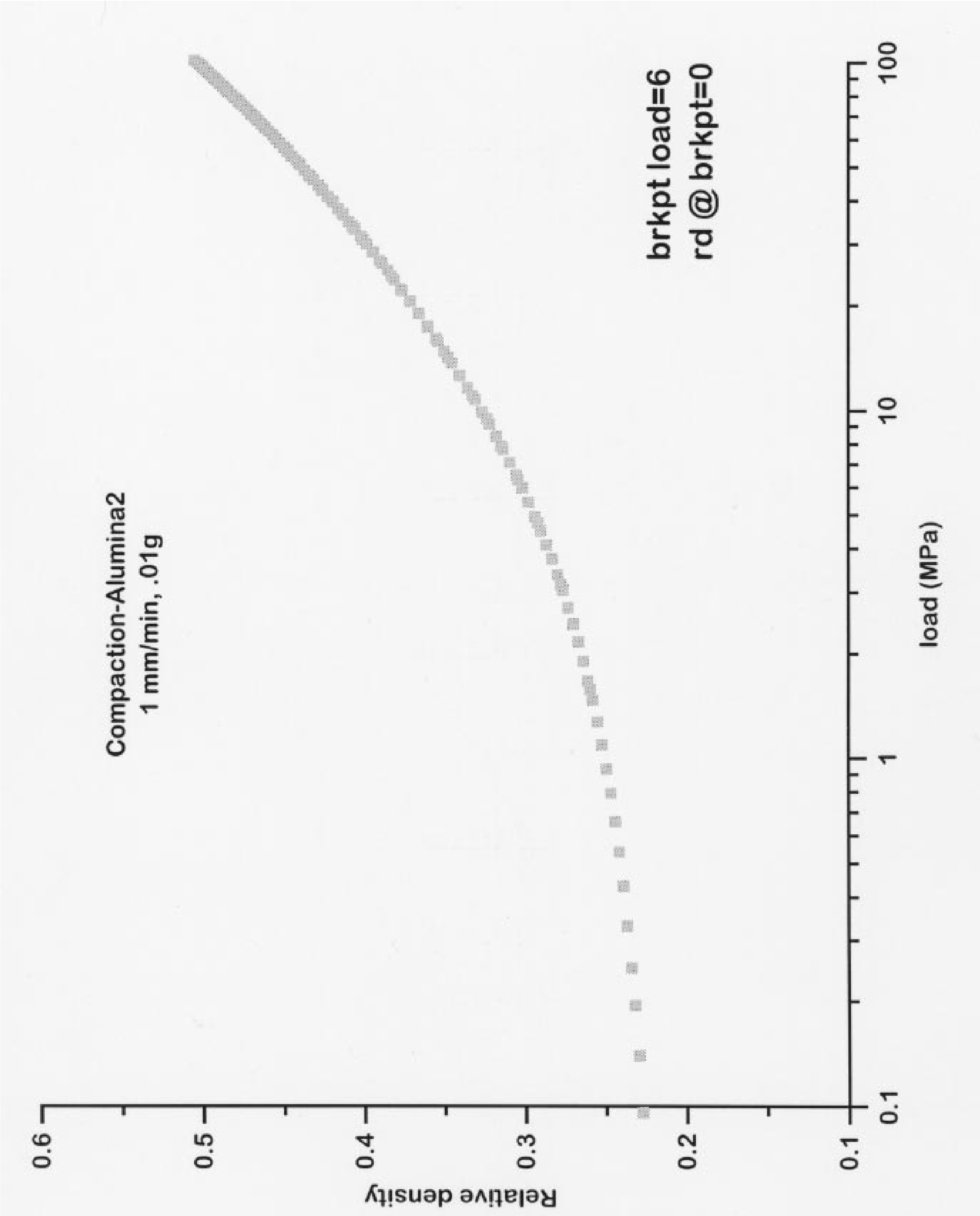

Fig. 2 Uniaxial compaction results for a second aliquot of the same alumina sample shown in Fig. 1. The compaction curve up to a pressure of 30MPa is very similar to that of fig. 1, however, using linear fits to the data at low and high pressures yields a breakpoint of 6 MPa.

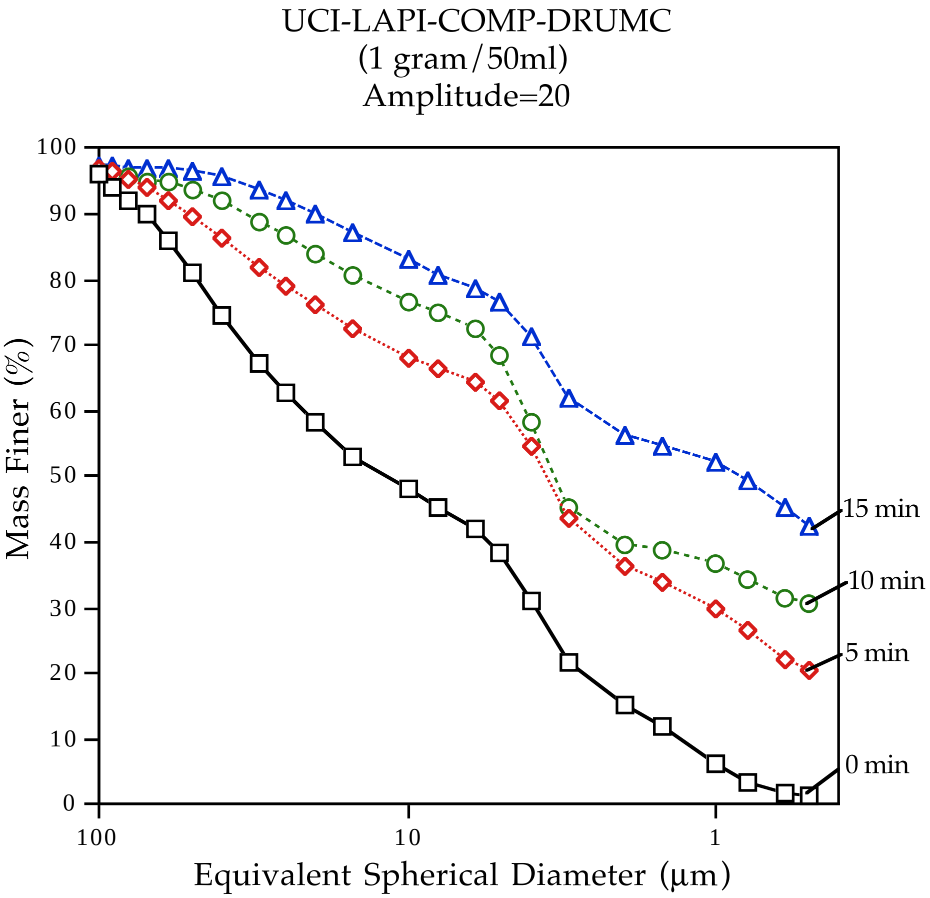

Fig. 3 Sedigraph particle size measurements for UCI F-T catalyst UCI-LAPI-COMP-DRUMC. The abscissa represents mass % of the sample finer than the indicated equivalent diameter. The sample represents a composite catalyst from the batch prepared for LaPorte run I. As seen from this figure, 15 minutes of ultrasound at a level of 20 causes considerable particle breakdown and generation of fine particles.

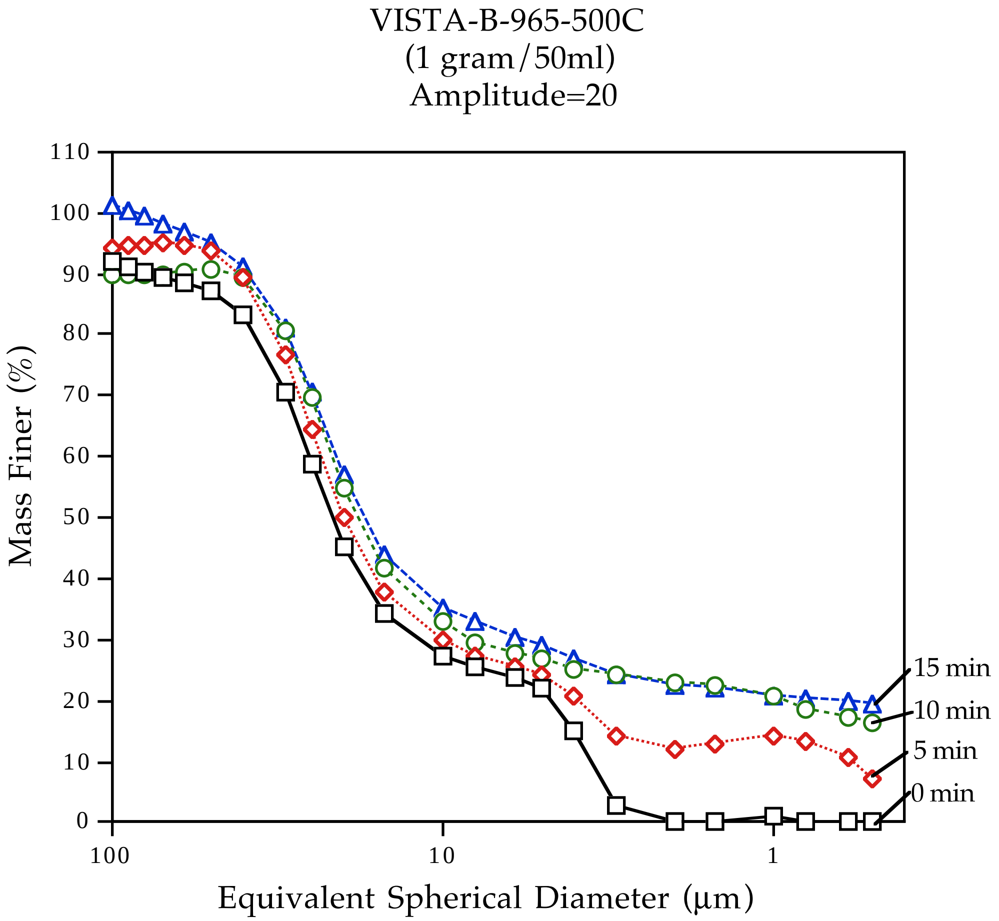

Fig. 4 Sedigraph particle size distribution of sample VISTA-B-965-500C obtained from Dr. RObert Gormley. The starting alumina from Vista was sieved and calcined in air at 500 °C. As seen from this figure, the alumina granules are much stronger than the catalyst shown in Fig. 3 and show very little fragmentation after 15 min of ultrasound irradiation.

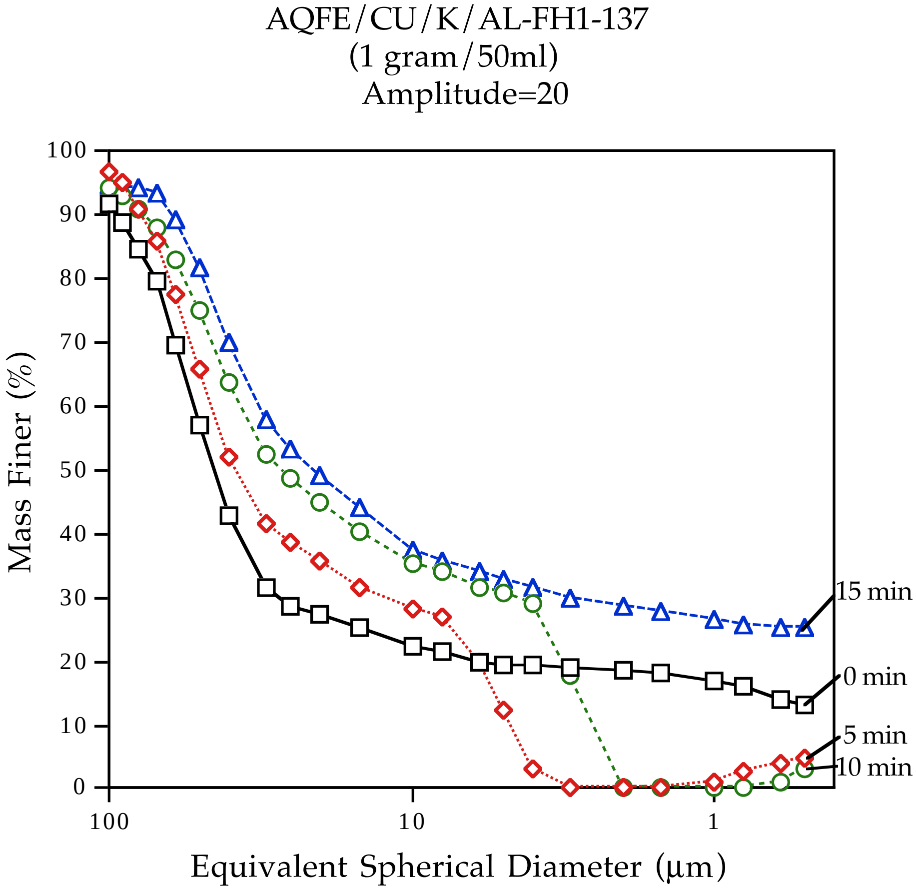

Fig. 5 Sedigraph particle size distributions of catalyst AQFE/CU/K/AL-FH1-137 which was prepared by Dr. Robert Gormley at PETC by impregnation of the Vista alumina (shown in Fig. 4). There appears to be some irreproducibility in the results with particles smaller than 10 µm. However, the extent of particle breakdown appears to be only marginally greater than the blank alumina sample.

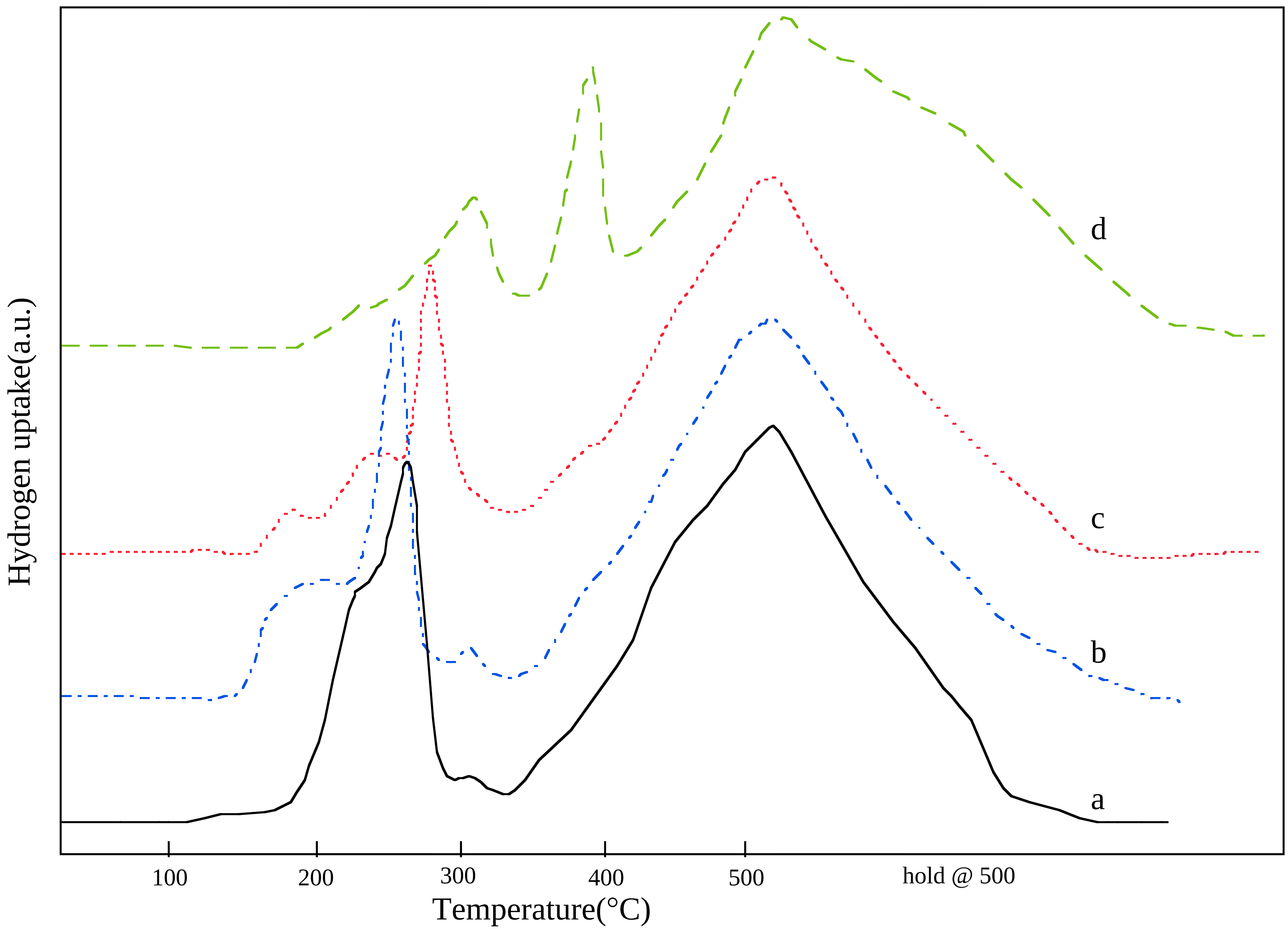

Fig. 6 `H_2-TPR results of UCI iron catalyst(1185-149) after preconditioning in argon flow
a. 150°C x 2 hours, b. 430°C x 1hour, c. 500°C x 1hour , d. 2nd-run H_2-TPR

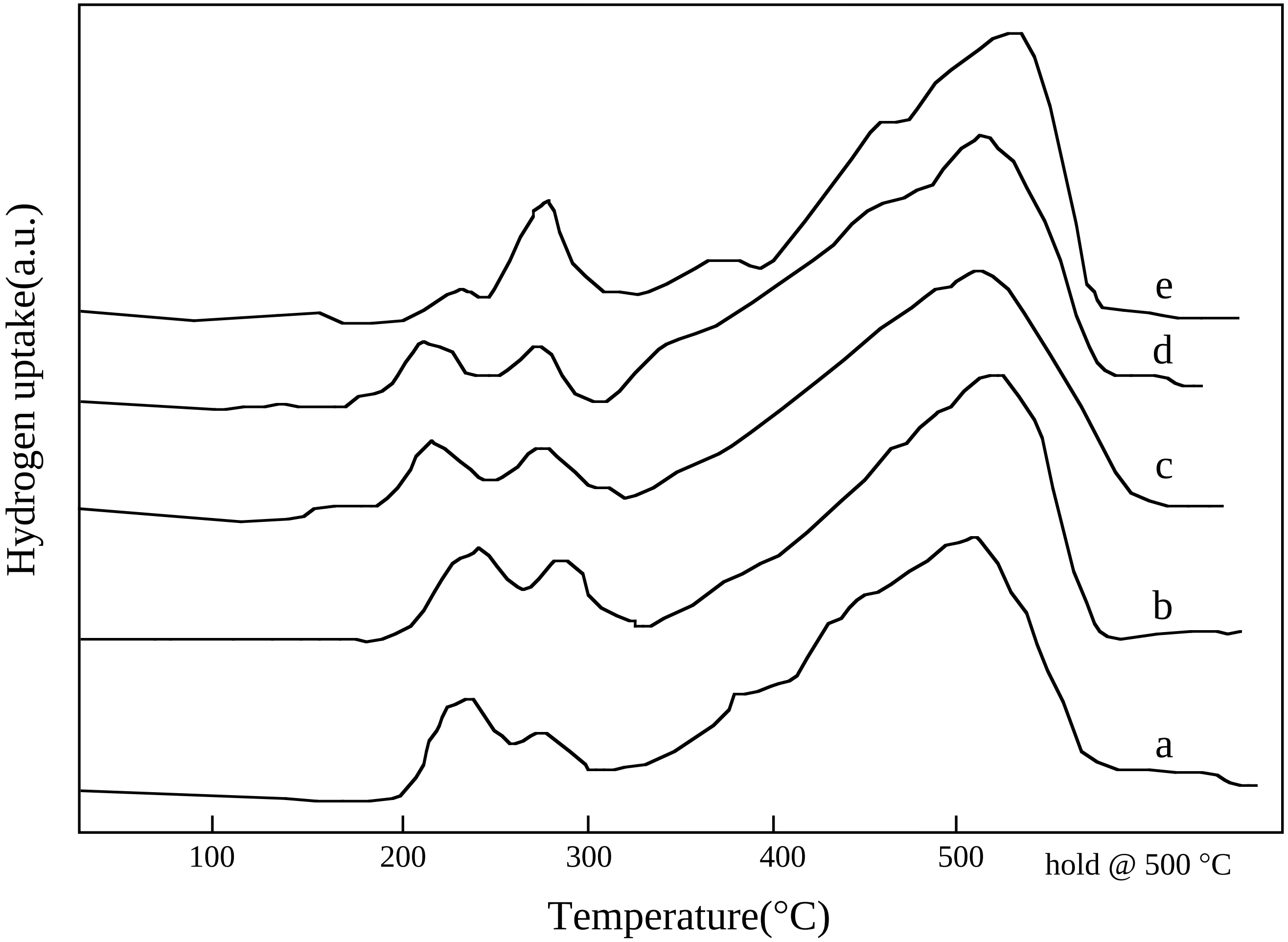

Fig. 7 H_2-TPR of YJ/1-65A(20 wt% Fe on silica sphere) after preconditioning in an argon flow
a. without preconditioning, b. 150°C x 2 hours, c. 430°C x 1hour,
d. 500°C x 1 hour, e. 2nd-run TPR

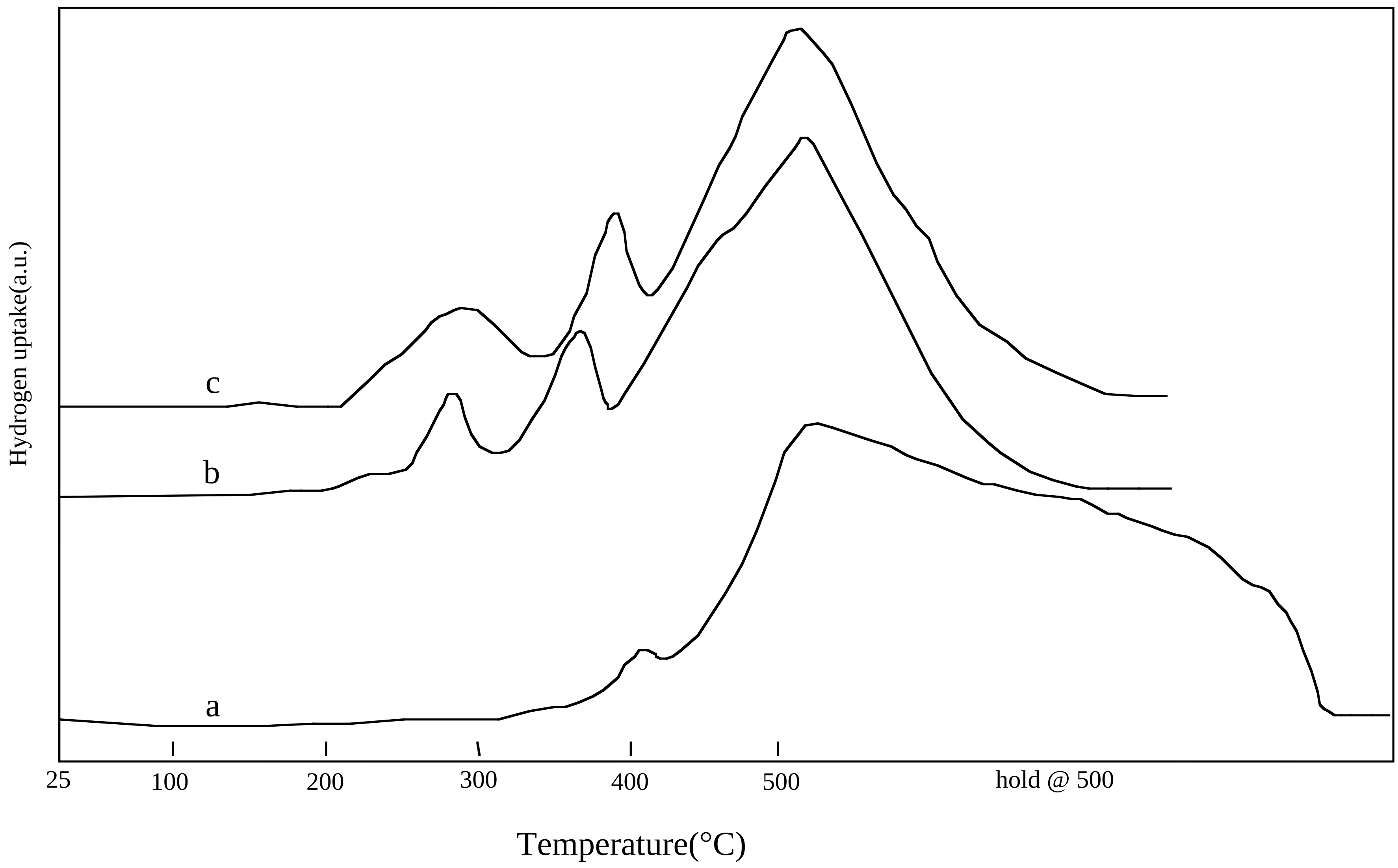

Fig.8. H_2-TPR of reference samples after preconditioning at 430°C for 1 hour
a. commercial magnetite, b. physical mixture of UCI 1185-149(50 wt%) and silica sphere
c. 2nd-run TPR of b

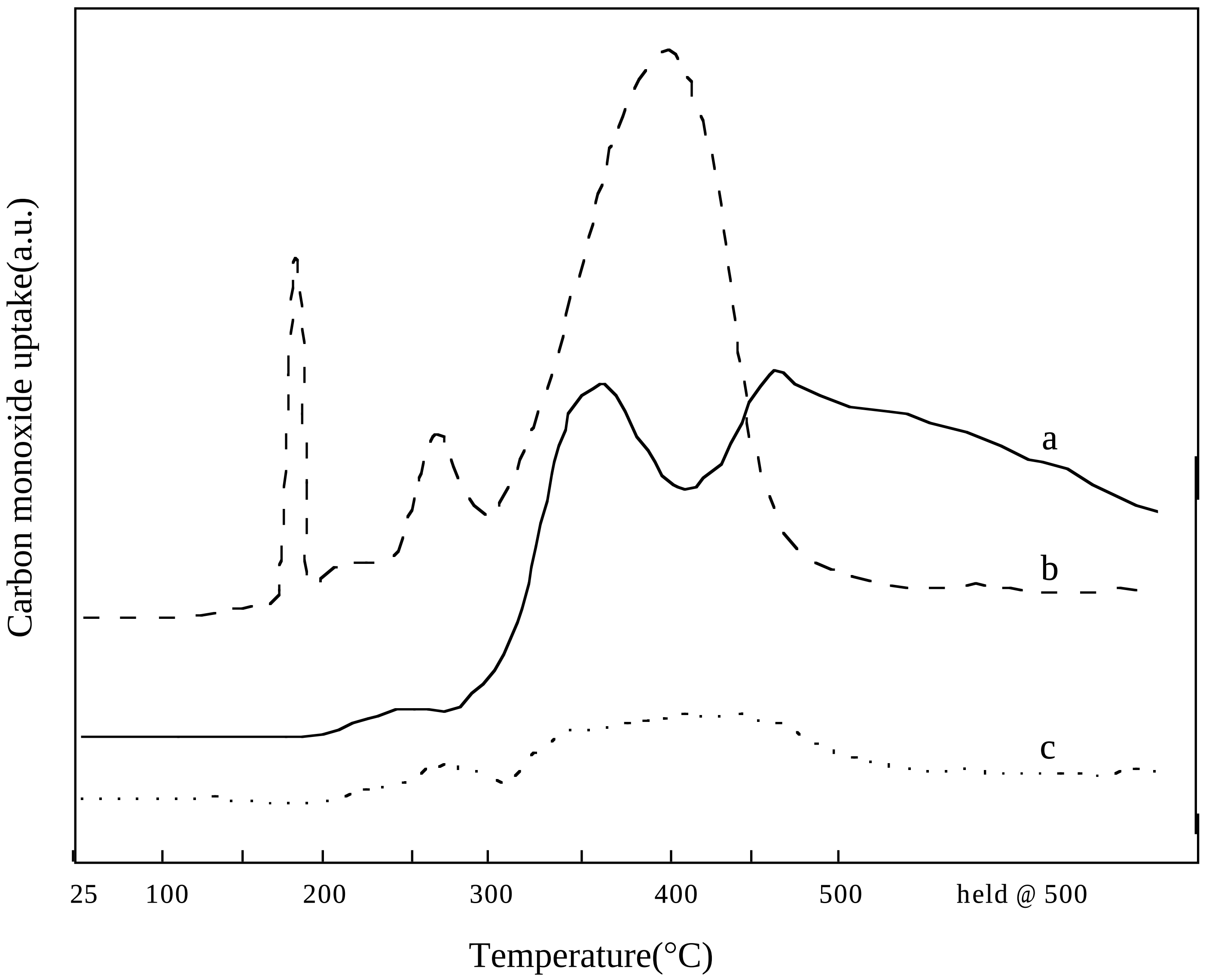

Fig.9. 1st-run CO-TPR results of iron catalysts

a. YJ/1-65A, b. UCI iron catalyst(1185-149), c. YJ/1-67(10 wt% Fe on silica sphere)

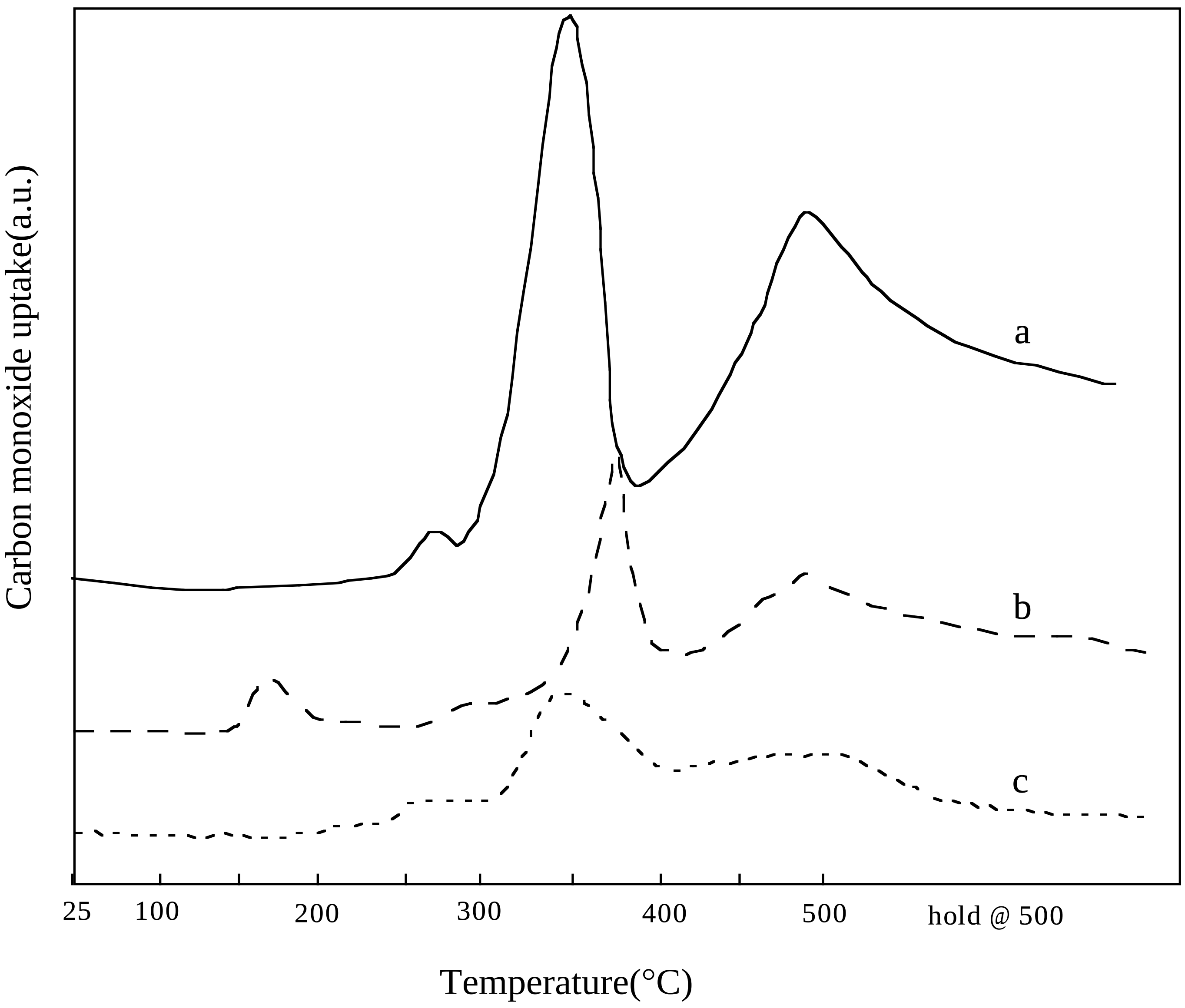

Fig. 10. 2nd -run CO-TPR results of iron catalysts

a. YJ/1-65A, b UCI catalyst, c. YJ/1-67

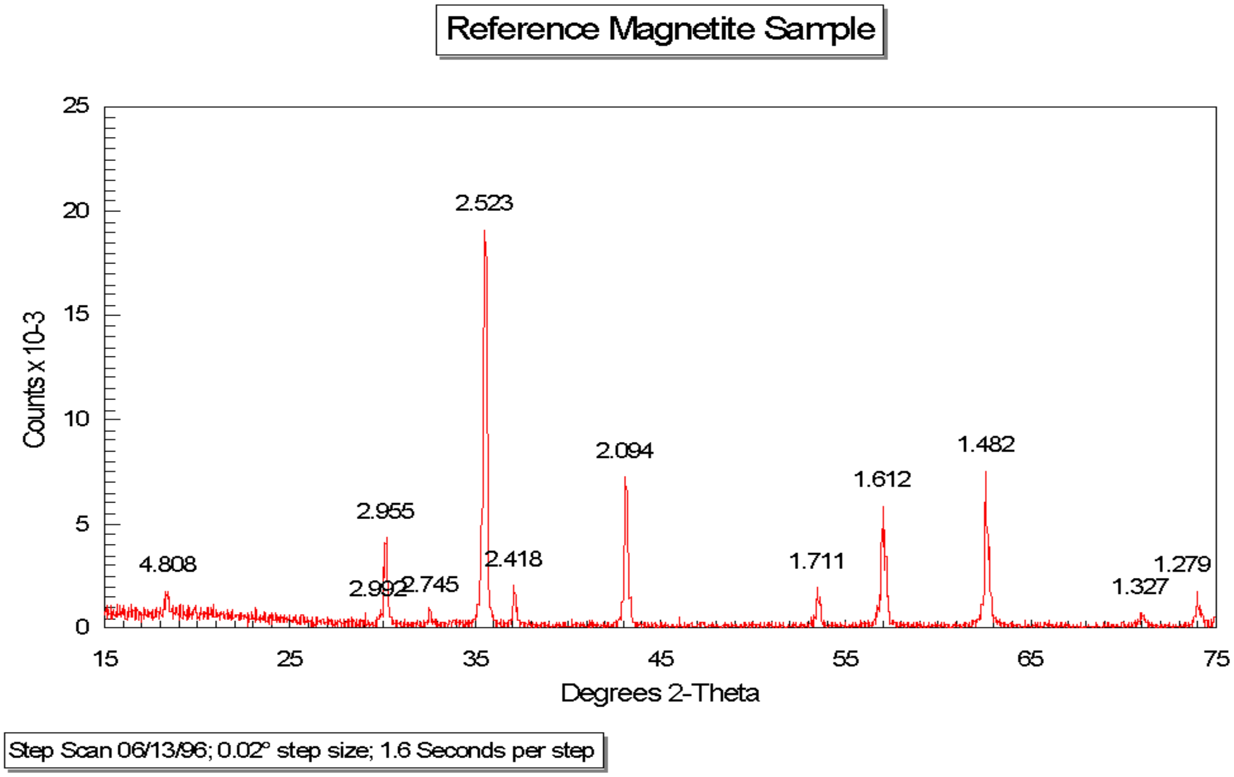

Step Scan 06/13/96; 0.02° step size; 1.6 Seconds per step

Figure 11. XRD pattern of natural magnetite

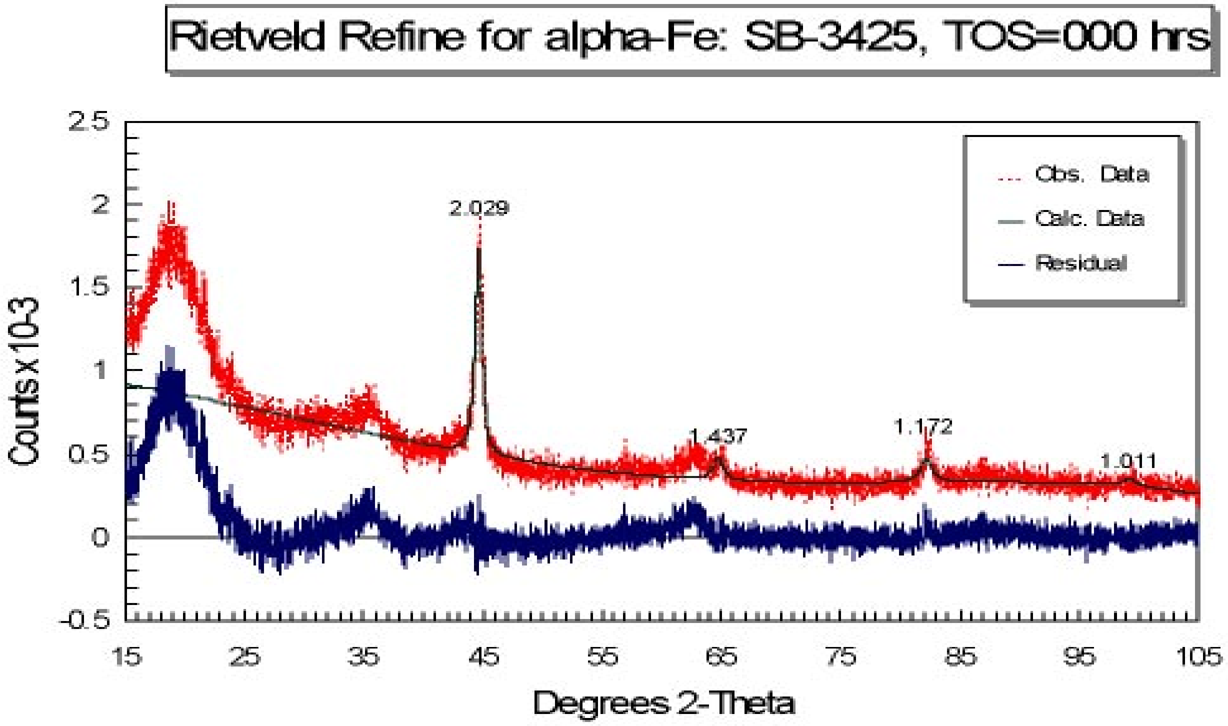

Fig. 12 XRD powder pattern of TAMU catalyst sample at time on stream = 0 hrs. Reitveld refinement shows that the primary constituent is α– Fe.

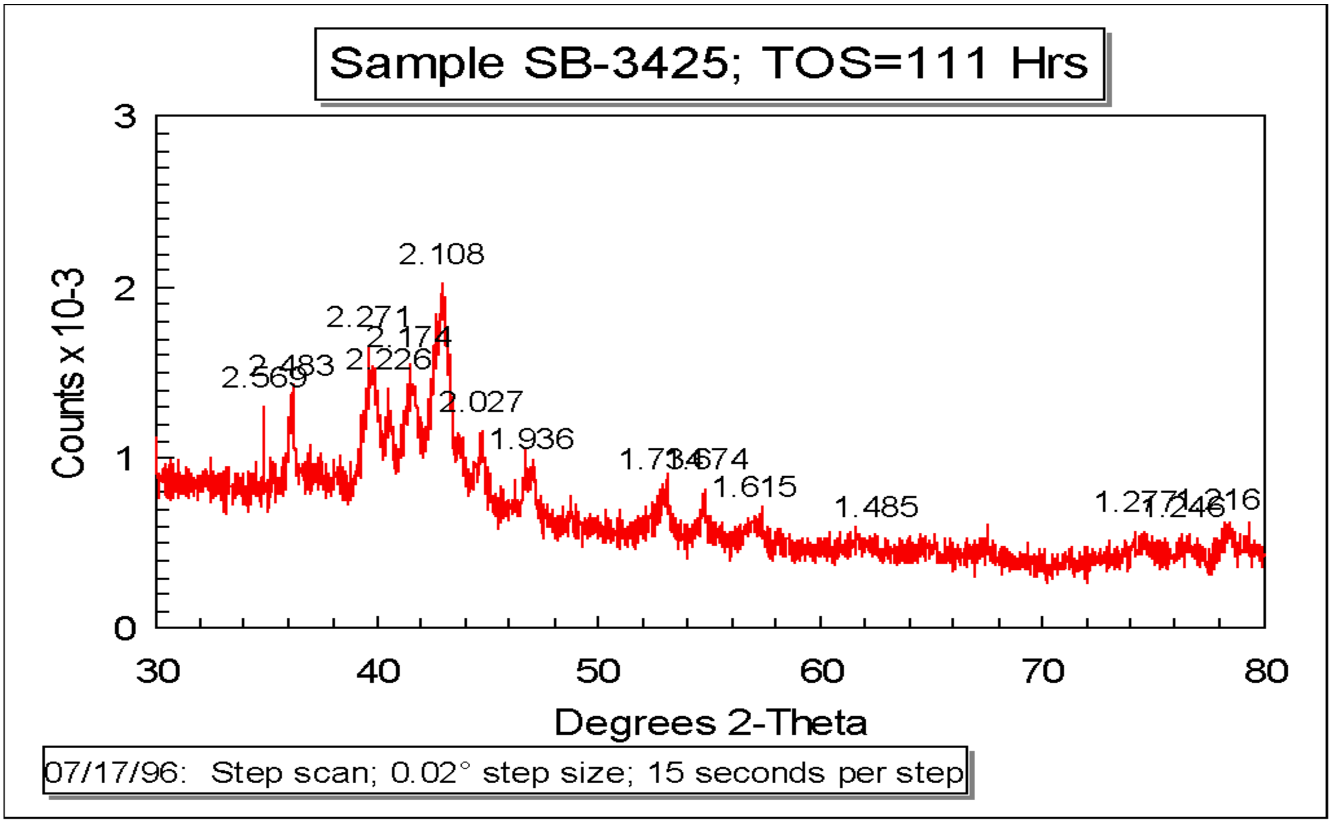
Sample SB-3425; TOS=111 Hrs

07/17/96: Step scan; 0.02° step size; 15 seconds per step

Figure 13 Sample of catalyst from run SB-3425 after 111 hours on stream. The prominent peaks can be attributed to the carbide phase. By analyzing the sample in wax, we prevent surface oxidation which occurs when the wax is stripped off.

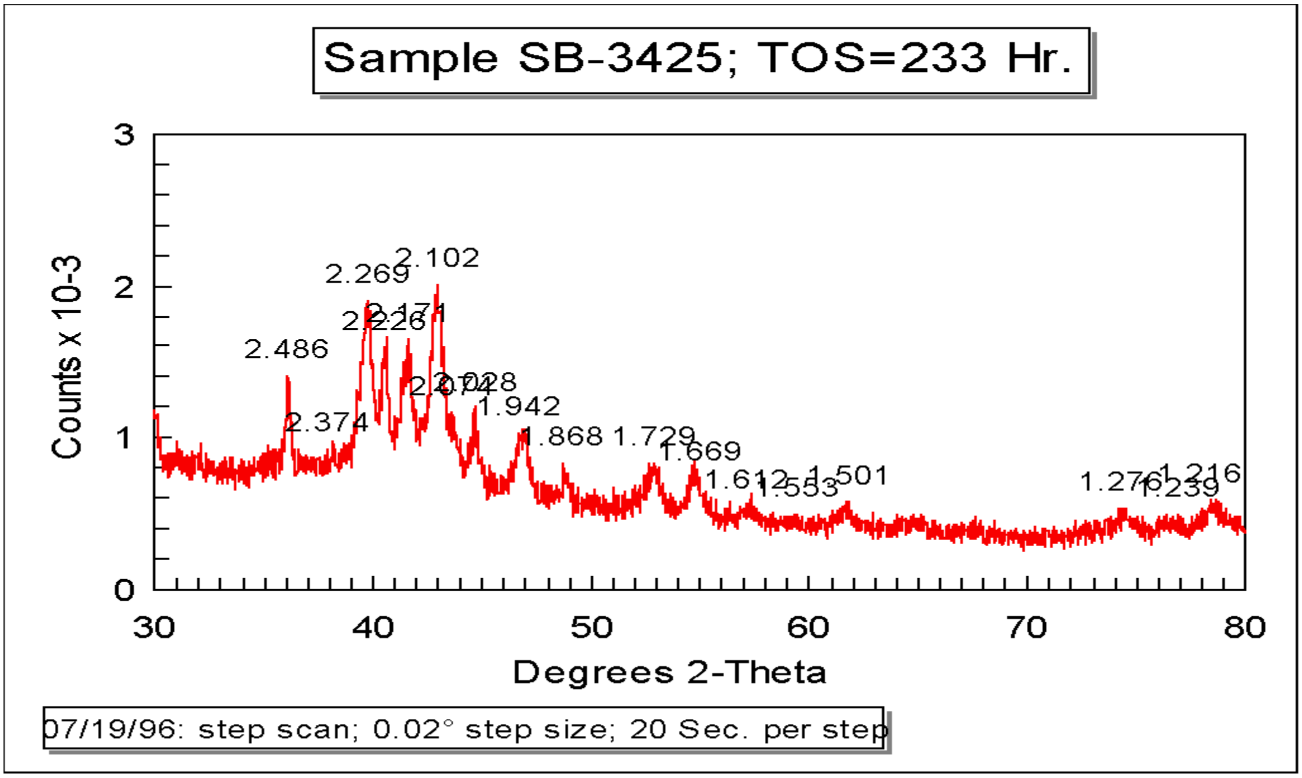
Sample SB-3425; TOS=233 Hr.

07/19/96: step scan; 0.02° step size; 20 Sec. per step

Figure 14 After 233 hours on stream, the carbide peaks grow in height indicating that the crystallinity of the sample has increased.

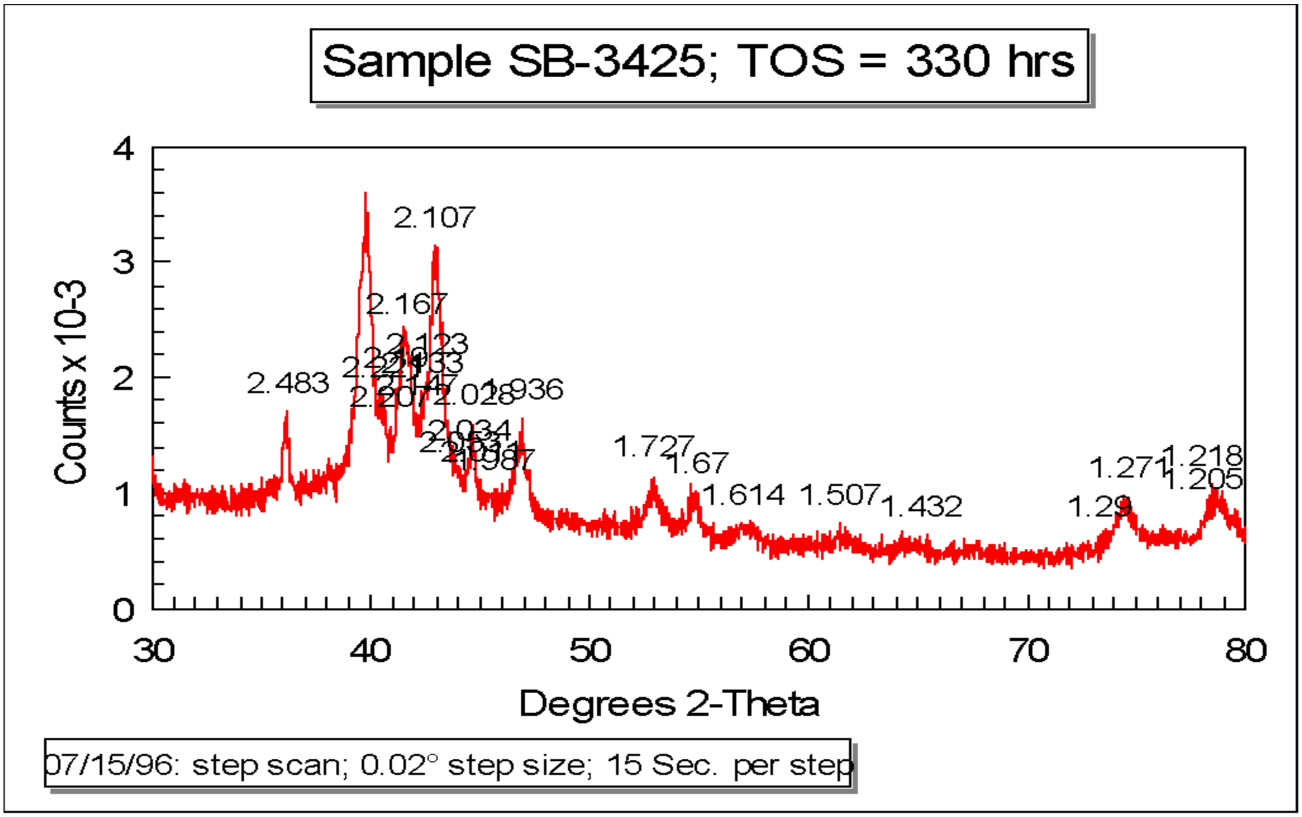

Figure 15 XRD pattern of catalyst after 330 hours on stream. The increased crystallinity of the carbide is seen in the growth of these peaks. There appears to be no transformation of carbide into magnetite.

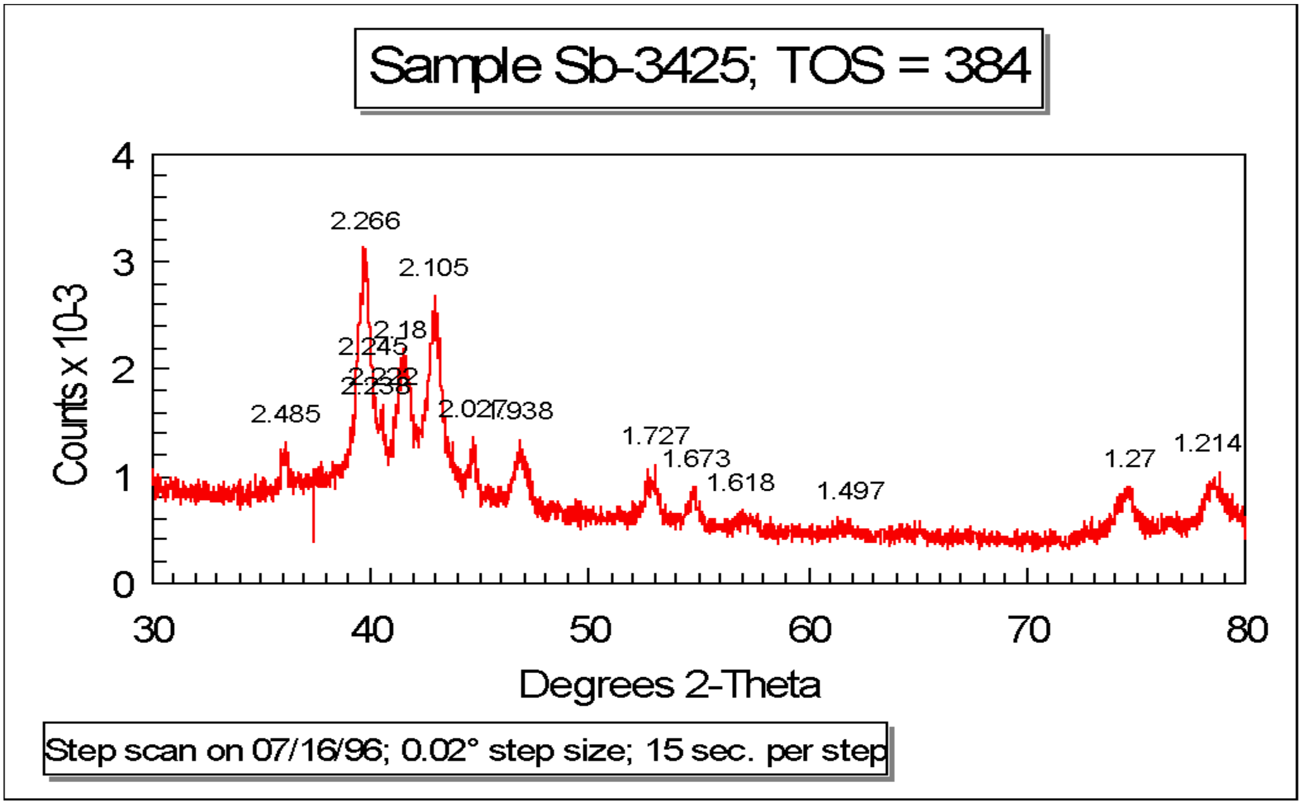

Figure 16 XRD pattern at end of run. Significant growth of the carbide peaks but negligible amounts of the magnetite phase seen over the course of this run.

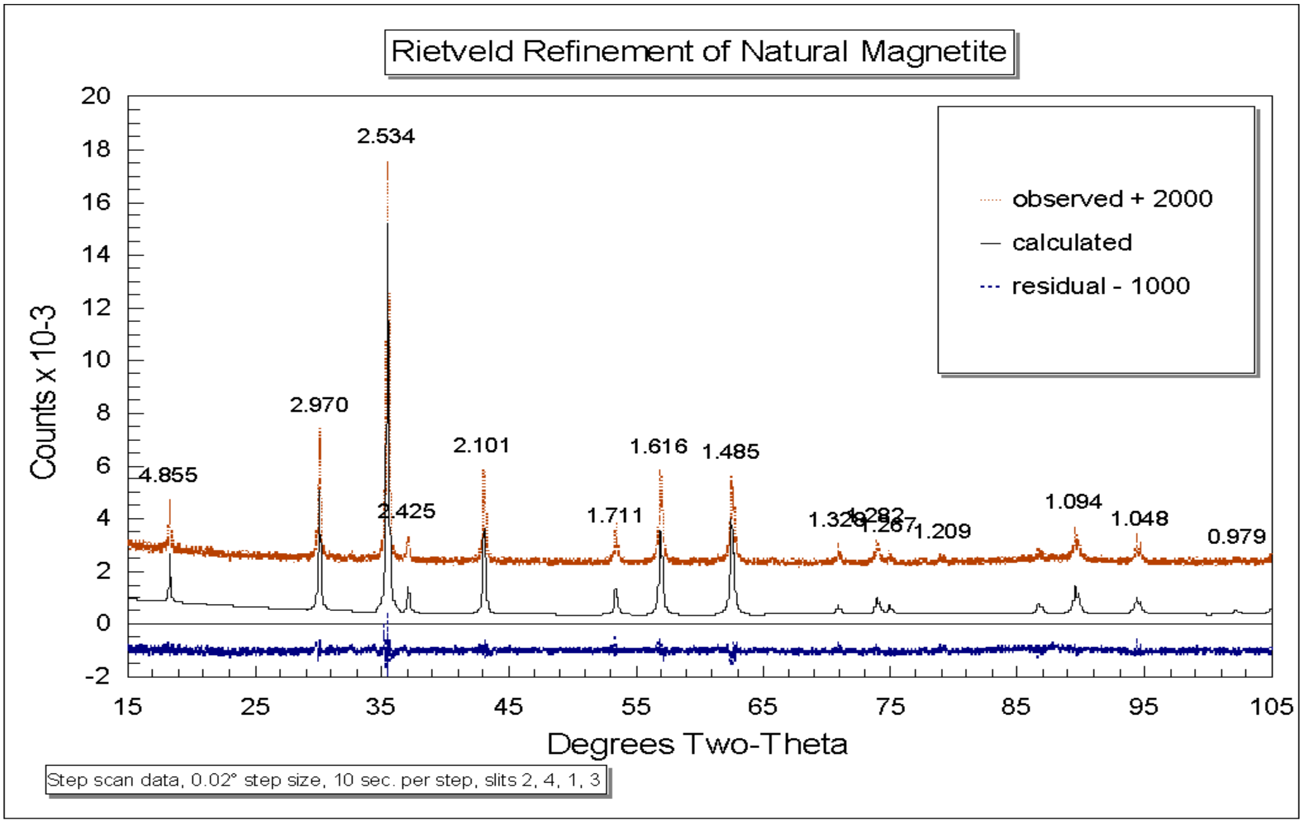

Fig. 17 Reitveld refinement of natural magnetite. The lowest curve shows the residual after subtracting the calculated pattern from the experimental one. It shows that the Reitveld method provides an excellent fit to the experimental data, accounting correctly for the intensities of the various peaks

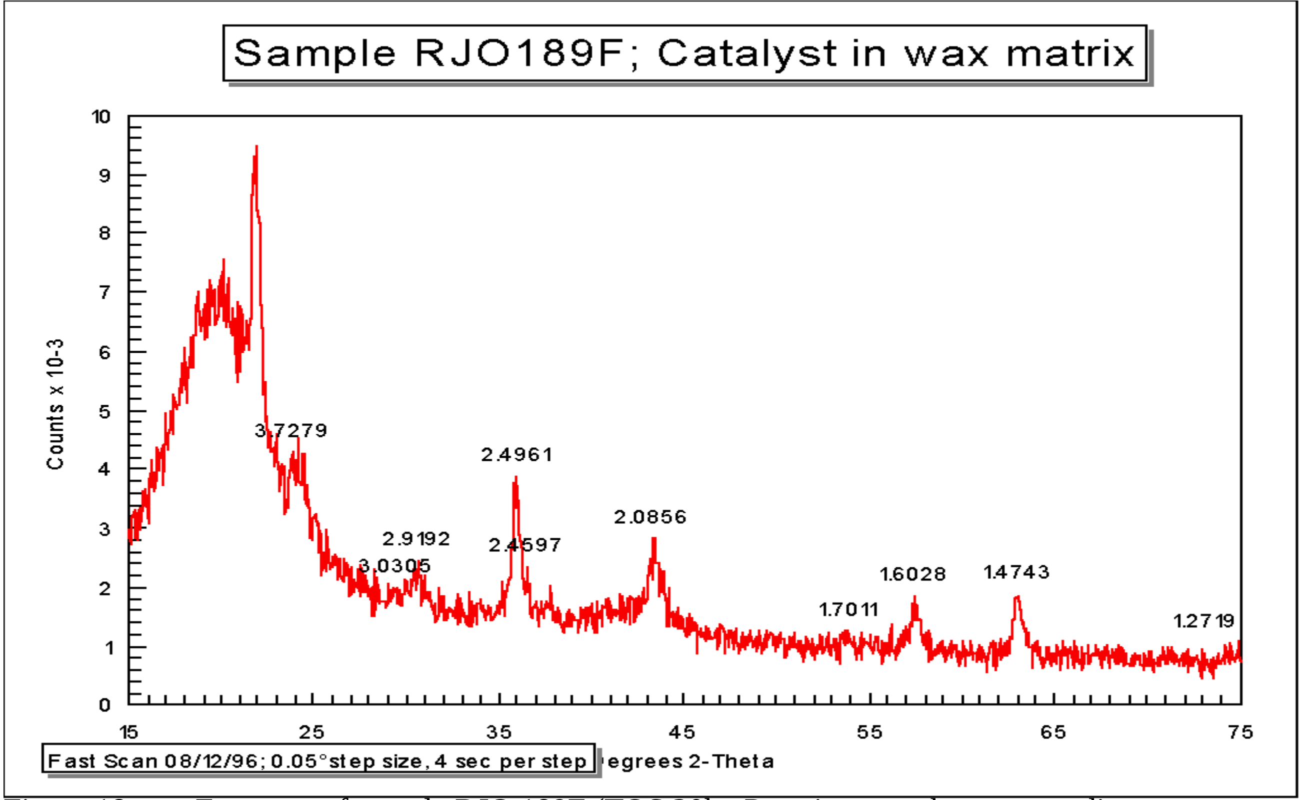

Figure 18 Fast scan of sample RJO 189F (TOS 20h. Prominent peak corresponding to magnetite is seen at 2.496 Å. However the size of the 2.0856 peak suggests the presence of carbide as well.

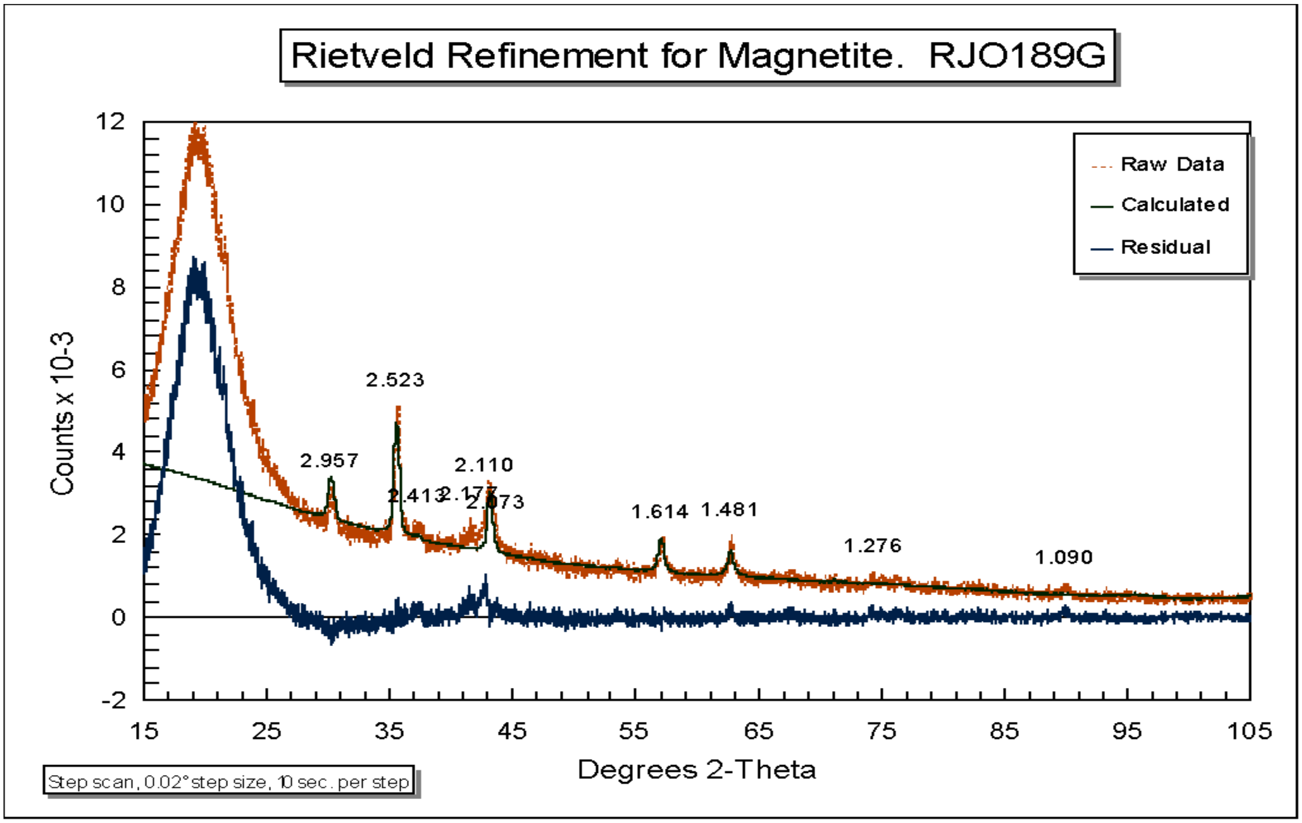

Figure 19 Reitveld refinement of sample RJO189G (TOS=122h) for magnetite. The residual after subtraction of magnetite is a a small peak corresponding to iron carbideas shown below.

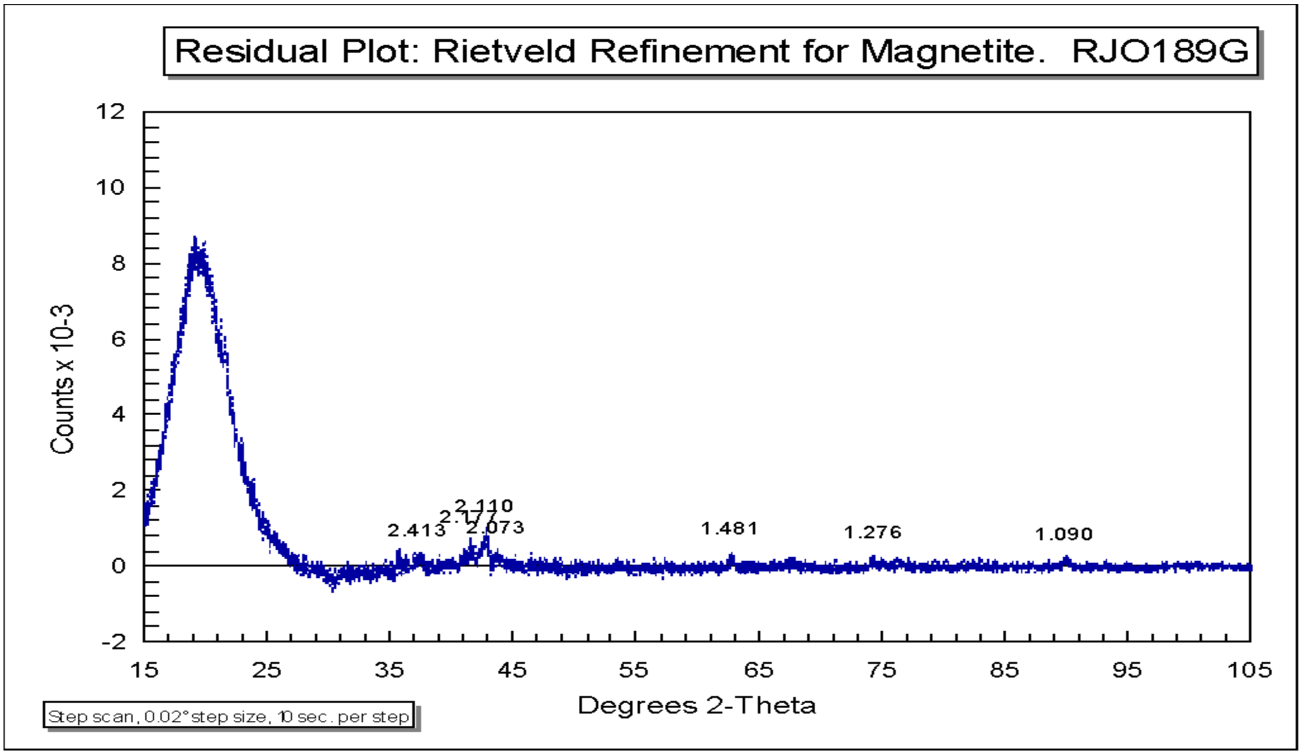

Figure 20 Residual after subtracting magnetite from the XRD powder pattern of sample RJO 189G

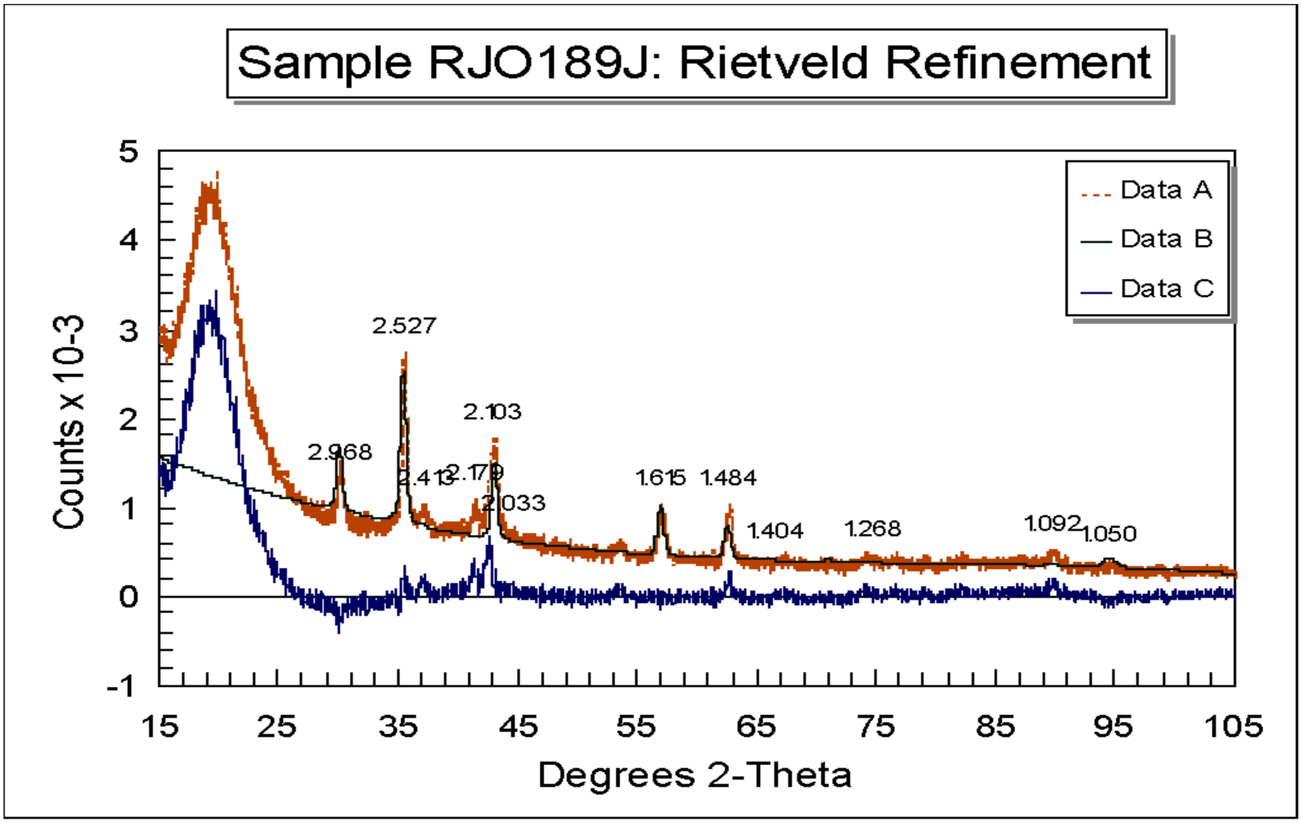

Figure 21 XRD powder pattern of RJO 189J (TOS 888h). Data A is the raw data, Data B is the refined pattern for magnetite and Data C is the residual.

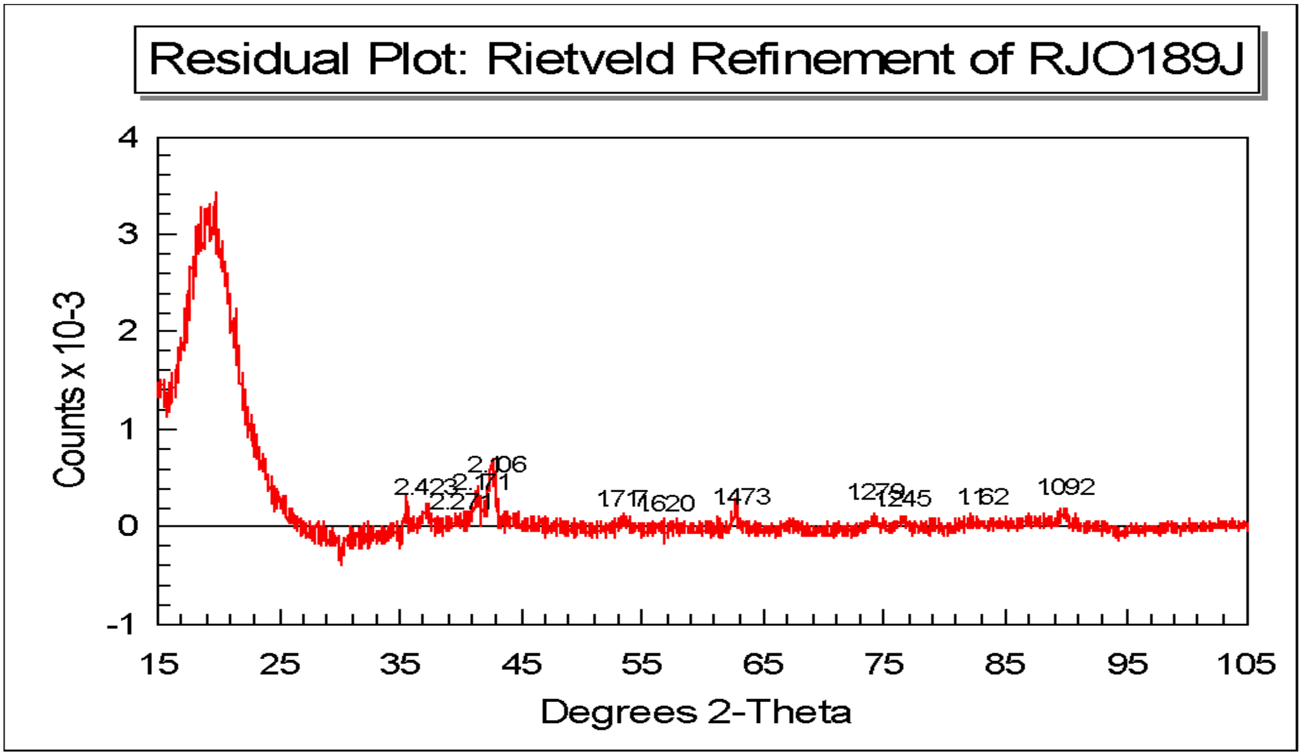

Figure 22 The residual after subtracting magnetite shows peaks corresponding to iron carbide.

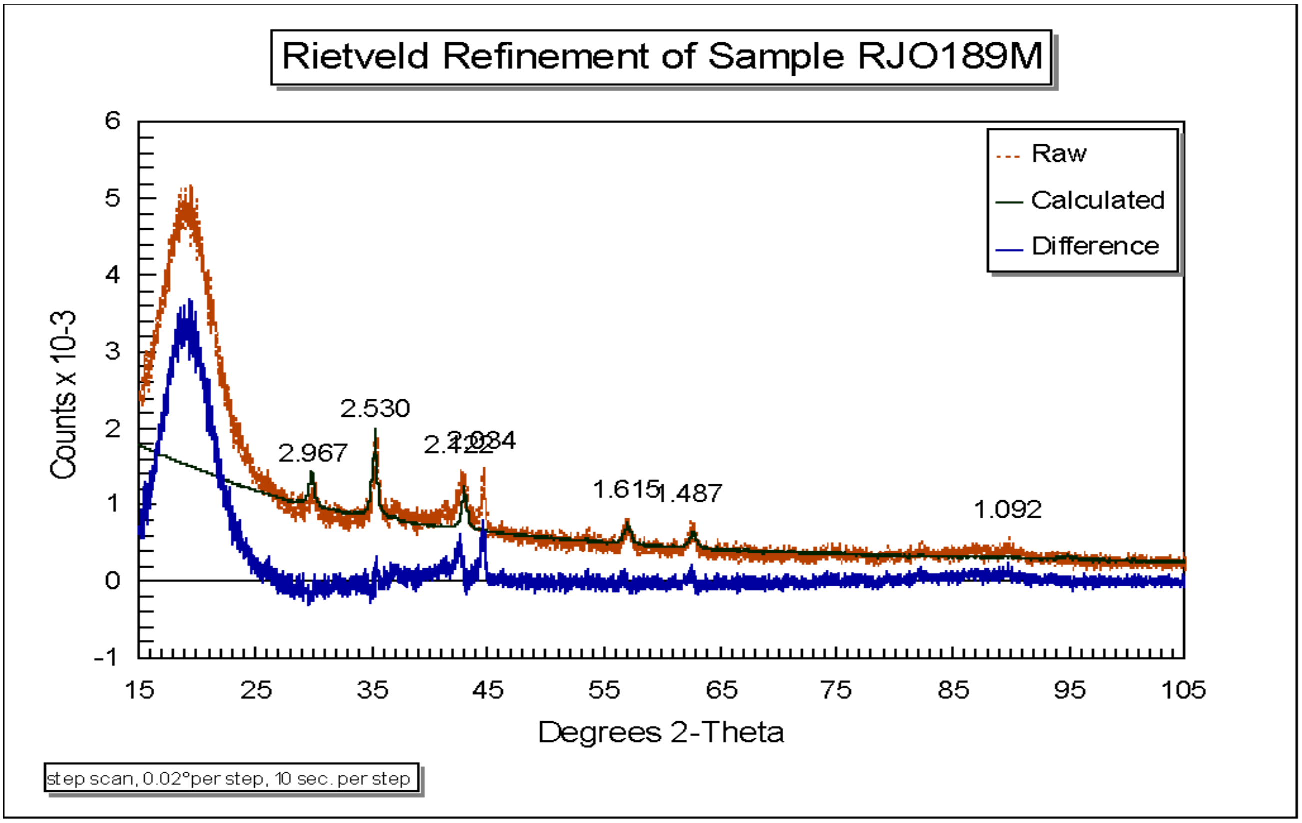

Figure 23 XRD powder pattern of sample RJO189 M showing how the Reitveld refinement for magnetite leaves behind a two peak pattern.

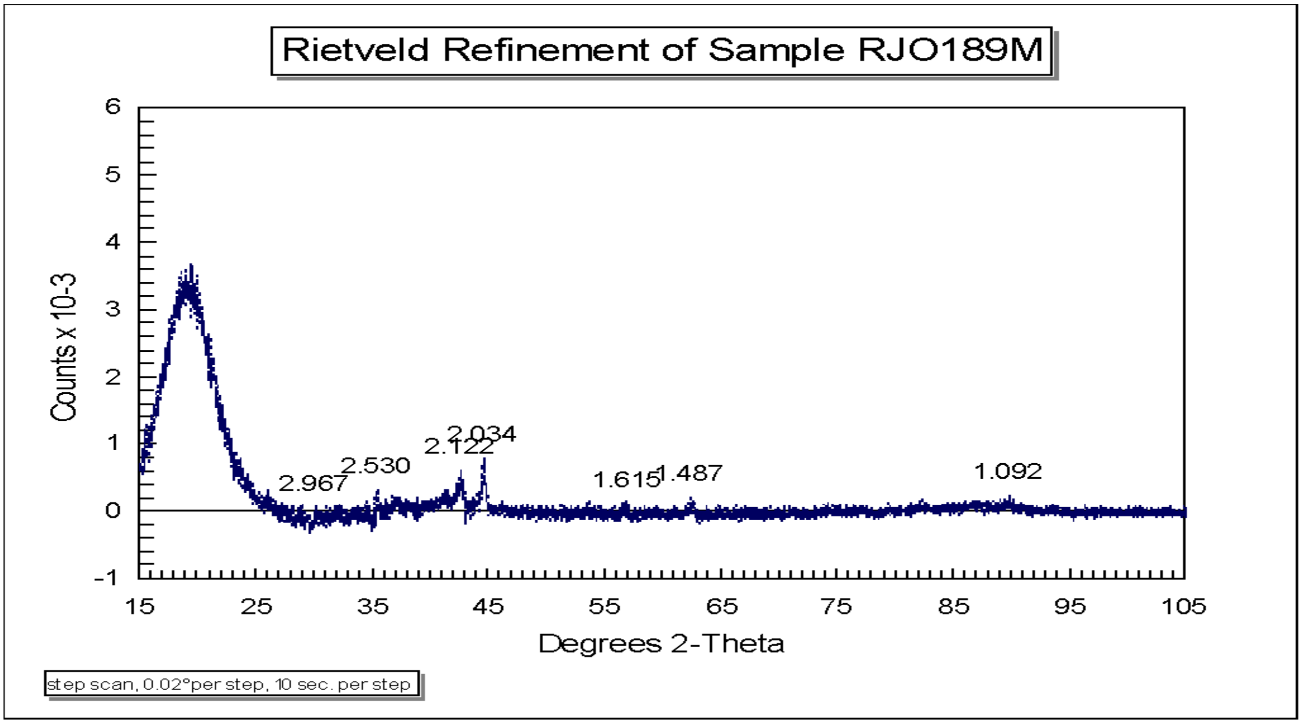

Figure 24 The residual from sample RJO 189M (TOS 1796h) shows two prominent peaks after the magnetite has been subtracted.

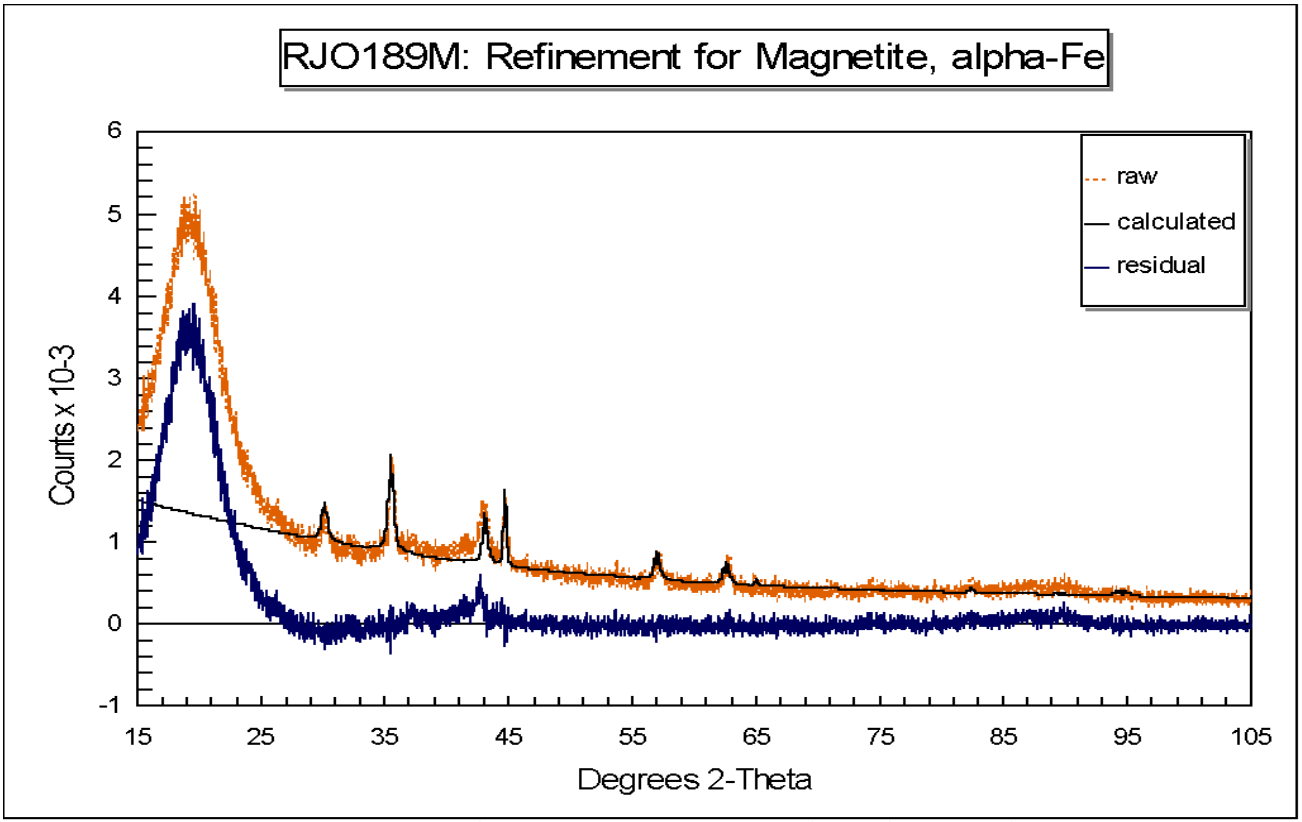

Figure 25 XRD powder pattern from sample RJO 189M after refinement for magnetite as well as α– Fe. The residual now shows peaks attributable to iron carbide.

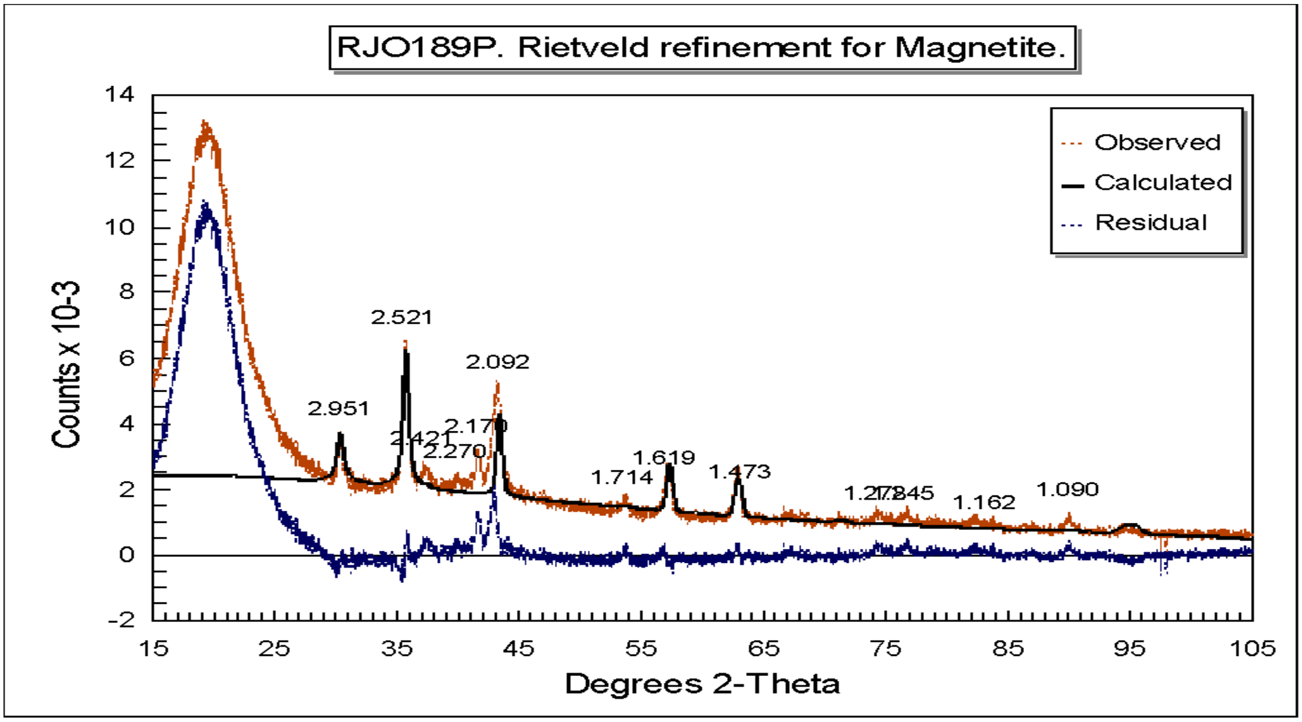

Figure 26 XRD powder pattern from sample RJO 189P (TOS = 3547h) after Reitveld refinement for magnetite.

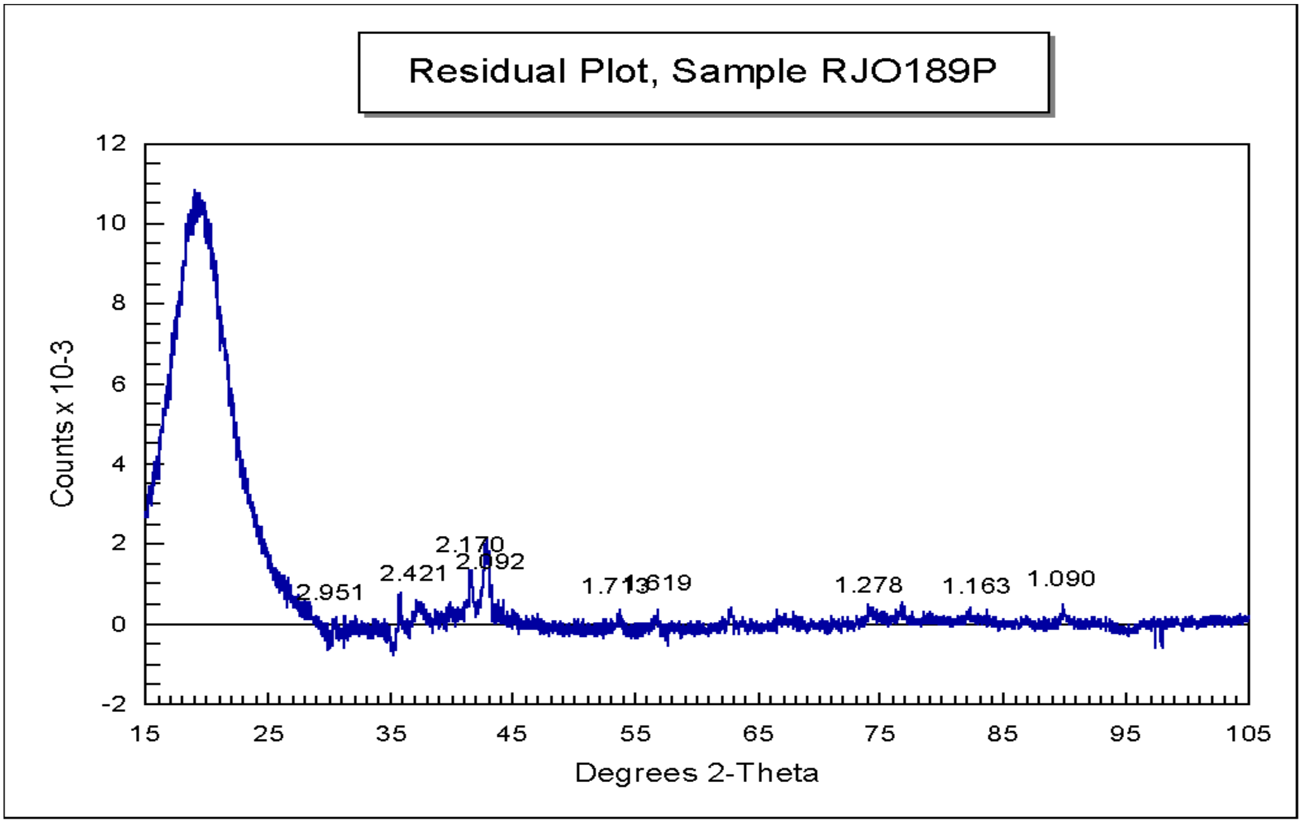

Figure 27 Residual plot from sample RJO 189P (TOS = 3547 h) after subtracting the magnetite peaks. A two peak pattern is seen, however the second peak does not match that for α– Fe.

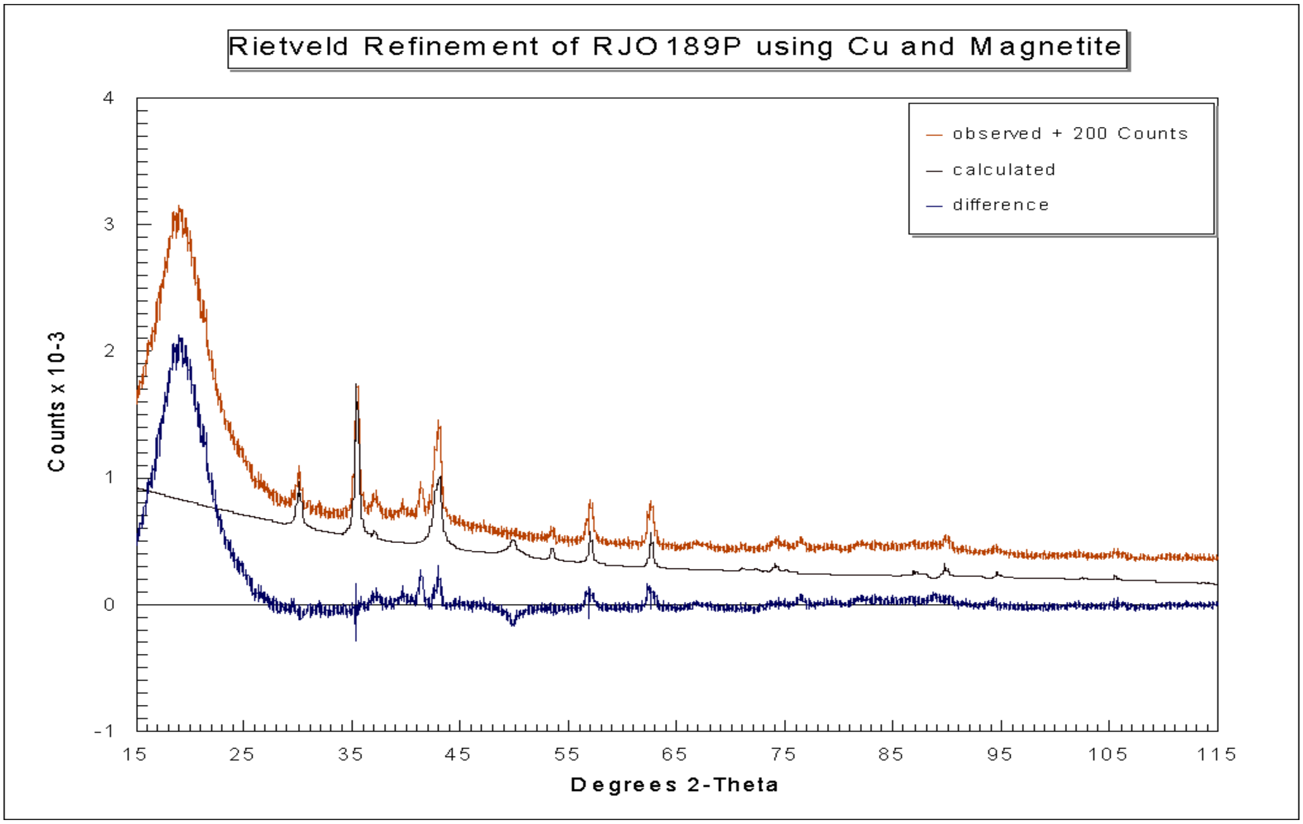

Figure 28 A trial fit was performed for metallic Cu, however, as shown here, subtraction of Cu yielded negative peaks in the residual showing that free Cu was not present in this sample.